MATERIALS CHEMISTRY FRONTIERS

CCS 中国化学会 CHINESE CHEMICAL SOCIETY

ICCAS

ROYAL SOCIETY OF CHEMISTRY

REVIEW

View Article Online
View Journal | View Issue

Cite this: *Mater. Chem. Front.*, 2021, **5**, 3257

Recent advances in PM6:Y6-based organic solar cells

Qing Guo,[a] Qiang Guo,[a] Yanfang Geng,[b] Ailing Tang,[b] Maojie Zhang, *[c] Mengzhen Du,[a] Xiangnan Sun [b] and Erjun Zhou *[b]

The last two years have witnessed rapid progress in organic solar cells (OSCs), driven by the newly-developed nonfullerene acceptor (NFA) Y6, which contains an electron-deficient core-based central fused ring. Inspired by Y6, a lot of novel Y-series NFAs with A–DA′D–A structures and matched polymer donors have been synthesized. Besides developing donor/acceptor materials, there are also many other factors contributing to the advances in OSCs. This review focuses on the most classic PM6:Y6 material combination and summarizes the recent progress in OSCs. First, the underlying mechanisms for the such high performance of OSCs based on PM6:Y6 are introduced. Then, the modifications of the active layer are discussed comprehensively, which involves incorporating a third monomer into PM6 to synthesize a terpolymer, towards the construction of ternary and quaternary devices, and various processing technologies. Next, the development of an interfacial layer and electrode materials in PM6:Y6-based OSCs are also summarized and discussed. Finally, perspectives and directions for the further development of OSCs are proposed.

Received 12th January 2021,
Accepted 18th February 2021

DOI: 10.1039/d1qm00060h

rsc.li/frontiers-materials

1. Introduction

As a promising energy conversion technology, organic solar cells (OSCs) have attracted wide attention due to their advantages, such as being low-cost, flexible, lightweight and semi-transparent.[1–5]

In general, OSCs consist of a transparent and conductive substrate, active layer, interfacial layers and electrodes. For high-performance OSCs, the active layer adopts a bulk heterojunction (BHJ) architecture, where a donor and an acceptor are mixed to form a bicontinuous network. Accurate control of proper phase separation guarantees highly efficient exciton separation and charge transport.[6–8] In recent decades, underpinned by the development of photovoltaic materials and device engineering, OSCs have seen rapid progress and their power conversion efficiencies (PCEs) have reached 16–18%.[9–17]

Developing novel photovoltaic materials has been one of the most important research areas in the past few decades. High-performance donor/acceptor photovoltaic materials should

[a] *Henan Institute of Advanced Technology, Zhengzhou University, Zhengzhou 450003, China*
[b] *CAS Key Laboratory of Nanosystem and Hierarchical Fabrication, CAS Center for Excellence in Nanoscience, National Center for Nanoscience and Technology, Beijing 100190, China. E-mail: zhouej@nanoctr.cn*
[c] *Laboratory of Advanced Optoelectronic Materials, College of Chemistry, Chemical Engineering and Materials Science, Soochow University, Suzhou 215123, China. E-mail: mjzhang@suda.edu.cn*

Qing Guo

Qing Guo is currently a lecturer at the Henan Institute of Advanced Technology, Zhengzhou University. She received her PhD degree from the College of Chemistry, Chemical Engineering and Materials Science of Soochow University in 2020. Her research interests focus on the synthesis and application of organic photovoltaic materials.

Qiang Guo

Qiang Guo received his PhD degree in 2019 from North China Electric Power University under the supervision of Prof. Zhan'ao Tan. He has been a lecturer at Henan Institute of Advanced Technology, Zhengzhou University since 2019. His present research interests include perovskite and organic solar cells.

fulfill several critical requirements: (1) good solubility for solvent processing, (2) strong and complementary absorption in the visible-near infrared region, (3) matched energy levels to strike a balance between the energetic offset for exciton separation and voltage loss, (4) high charge mobility, which is usually 10^{-5}–10^{-4} cm^2 V^{-1} s^{-1} and measured using the space charge limited current (SCLC) method, and (5) suitable aggregation performances and miscibility between the donor and acceptor to form nanoscale phase separation. Before 2015, acceptor materials were dominated by fullerenes due to their unique performance in terms of high electron affinity and mobility. However, the deficiencies of fullerenes, such as their weak absorption, difficult modification and easy dimerization, result in the theoretical efficiency of fullerene-based OSCs being limited to ~13%.[18,19] Afterwards, the nonfullerene acceptors (NFAs) were strongly investigated to solve these problems and effectively overcome the trade-off between the short circuit current (J_{SC}) and open circuit voltage (V_{OC}).[20–27]

In terms of chemical structure, NFAs with a acceptor–donor–acceptor (A–D–A) type structure, which consists of an electron-donating fused-ring core as the D unit, and electron-withdrawing end groups as the A unit, have been widely studied and exhibit excellent photovoltaic performance. OSCs based on A–D–A-type NFAs have reached high PCEs of over 15%, with a general efficiency of around 13–14% for single-junction devices.[28–33] In 2019, a novel NFA Y6 with a A–DA′D–A structure was developed, as shown in Fig. 1, where an electron-deficient core-based central fused ring was used.[34] When paired with the widely used polymer donor PM6, the Y6-based OSCs delivered a high PCE of 15.7% with a simultaneously high V_{OC} (0.825 V), J_{SC} (25.2 mA cm^{-2}) and fill factor (FF, 74%), which is one of the important milestones in the progress of OSCs. Under the induction of Y6, a series of Y-series derivatives were developed by modifying the electron-deficient core,[35,36] alkyl chains,[10,37] and end groups[11,13] to tune the solubility and aggregation performance of the NFAs. In addition, novel polymer donors

Yanfang Geng

Yanfang Geng received her PhD degree in Materials Science from the Beijing Institute of Technology in 2012 under the supervision of Prof. Wenhui Wu. From 2009 to 2011, she studied at The University of Tokyo with Prof. Kazuhito Hashimoto and Prof. Keisuke Tajima as a Joint Training doctoral student. In 2012, she joined the National Center for Nanoscience and Technology (NCNST), China, as an assistant professor. In 2016, she was promoted to associate professor. Her research interests are the design and self-organization of organic functional materials for optoelectronic applications.

Ailing Tang

Ailing Tang received her PhD degree in physical chemistry from the Institute of Chemistry, Chinese Academy of Sciences (ICCAS) in 2005. She is currently an associate professor at the CAS Key Laboratory of Nanosystem and Hierarchical Fabrication, National Center for Nanoscience and Technology (NCNST), China. Her research interests include the design of photovoltaic materials for high-voltage organic solar cells and the exploration of the related device mechanism.

Maojie Zhang

Maojie Zhang is a professor in the College of Chemistry, Chemical Engineering and Material Science at Soochow University. He received his PhD in physical chemistry from the Institute of Chemistry, Chinese Academy of Sciences (ICCAS) in 2011 and continued to work as an assistant professor in ICCAS with Prof. Jianhui Hou. He joined Soochow University as a full Professor in 2014. His research interests focus on photovoltaic materials and devices for polymer solar cells.

Erjun Zhou

Erjun Zhou received his PhD degree in chemistry from the Institute of Chemistry, Chinese Academy of Sciences (ICCAS) in 2007 under the supervision of Prof. Yongfang Li. From 2007 to 2014, he worked in Japan with Prof. Kazuhito Hashimoto and Prof. Keisuke Tajima as a postdoctoral fellow/research scientist at the JST, the University of Tokyo and RIKEN. In 2014, he joined the National Center for Nanoscience and Technology (NCNST), China, as a full professor. His research interests are the design, synthesis, and characterization of organic and polymeric functional materials for optoelectronic and photovoltaic applications.

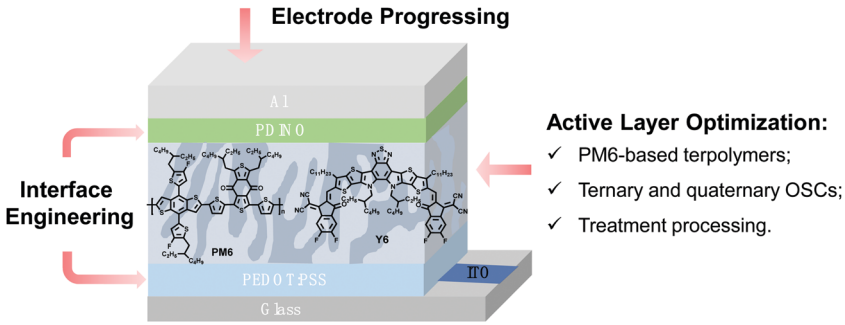

Fig. 1 Schematic diagram of the main content of this review.

have also been developed simultaneously to pair with Y6.[14,15,38–43] As a result, the field has seen excellent progress, with a PCE of around 18% achieved for single-junction OSCs, and corresponding reviews have been published recently.[44–52]

In fact, PM6 (also named PBDB-TF, PBDB-T2F) is a D–π–A type copolymer (as shown in Fig. 1), with an optical bandgap of ≈1.80 eV and a highest occupied molecular orbital (HOMO) energy of ≈−5.50 eV, where benzodithiophene (BDT), thiophene, and benzodithiophene-4,8-dione (BDD) served as the D, π, and A units, respectively.[53] PM6 has been proved to be a star polymer donor and can be widely used to blend with different NFAs, including both small molecules[54–57] and polymers.[58–60] As the most classic donor and acceptor material, PM6:Y6-constructed devices have attracted a lot of study. On the one hand, ternary OSCs, thermal/solvent annealing and additive processing have been developed to optimize the morphology of the active layers and further improve the PCE. On the other hand, the interfacial layers and electrodes have also been investigated for achieving efficient carrier transport and extraction, thereby leading to high photovoltaic performance, as well as meeting the requirements of practical commercial applications. Systematic understanding of this work is helpful for us to further understand the relationship among the molecular characteristics, active layer morphology, device physics and photovoltaic performance.

Hence, in this review, we discuss the development of OSCs based on PM6:Y6 in three parts, as summarized in Fig. 1. First, the underlying mechanisms for the such high performance are analyzed. Then, a comprehensive description of bulk heterojunction (BHJ) layer optimization is presented, including: (1) the design and development of new terpolymers based on PM6, (2) ternary and quaternary OSCs, (3) various treatments such as solvent/solid additive processing. Next, the recent progress of interfacial layers and electrodes in PM6:Y6-based OSCs is discussed. This review is intended to help researchers keep abreast of the recent achievements, and gain inspiration for the development direction of high-performance OSCs. Here, it should be noted that effectively comparing photovoltaic efficiencies made in different research groups is challenging due to factors such as the influence of the light source and the definition of the active area of OSCs.[61,62] In addition, the accuracy of the PCE may be limited by measurement techniques, with the error expected to be in the of range 3–5%.[63,64] Therefore, the PCE values in this review are presented in the form of three significant figures. Note that it is the optimization strategy that deserves more attention, but not the accuracy of the PCE.

2. Underlying mechanisms for the high performance of PM6:Y6 OSCs

According to the reported literature,[34] Y6 exhibits complementary absorption to PM6, with an absorption onset of 931 nm and absorption coefficient of 1.07×10^5 cm^{-1}, as shown in Fig. 2. The HOMO and LUMO energy levels of Y6 are calculated to be −5.65 and −4.10 eV, which match those of PM6. The external quantum efficiency (EQE) spectrum of the PM6:Y6-based device shown in Fig. 2d demonstrates its broad photoresponse, extending from 300 to 900 nm, which is in good agreement with the absorption spectroscopy results.

To understand the underlying origin of the excellent performance of PM6:Y6-based OSCs, the V_{OC}, J_{SC} and FF values of the devices have been analyzed systematically. First, delving deeper into the energy losses (E_{loss}) is beneficial for understanding high V_{OC} values. As reported,[65] the total E_{loss} ($E_{loss} = S_1 - qV_{OC}$, where, S_1 is the singlet exciton energy of the lower bandgap component in the blend and q is the elementary charge) was calculated to be 0.535 eV, with a low driving force ($\Delta E_{S1,CT}$, energy difference between S_1 and charge transfer state, CT) of 0.05 eV, radiative recombination (ΔE_{rad}) of 0.199 eV and non-radiative recombination ($\Delta E_{non\text{-}rad}$, calculated from $k_BT\ln(EQE_{EL}^{-1})$, where EQE_{EL} is the EQE of the electroluminescence, measured to be 1.3×10^{-5} as shown in Fig. 2e) of 0.286 eV, which are among the lowest values reported in the literature.[66,67] The corresponding parameters are indicated in Fig. 2f. In addition, the E_{loss} from energetic disorder was calculated to be as low as 26.7 meV. As Durrant *et al.* reported,[68] the low energetic disorder caused by the tail state could be due to the high degree of conformational rigidity and uniformity for Y6, as a result of the presence of the two alkyl side chains on the outer core.

Even though there is a small energetic offset of the highest occupied molecular orbital (HOMO) between the donor and acceptor, the PM6:Y6-based devices show efficient hole transfer, leading to high performance. Previous studies proposed several mechanisms such as "hot" CT states and entropy-driven charge separation (CS).[69–71] Recently, barrier-free CS was proposed.[72–74]

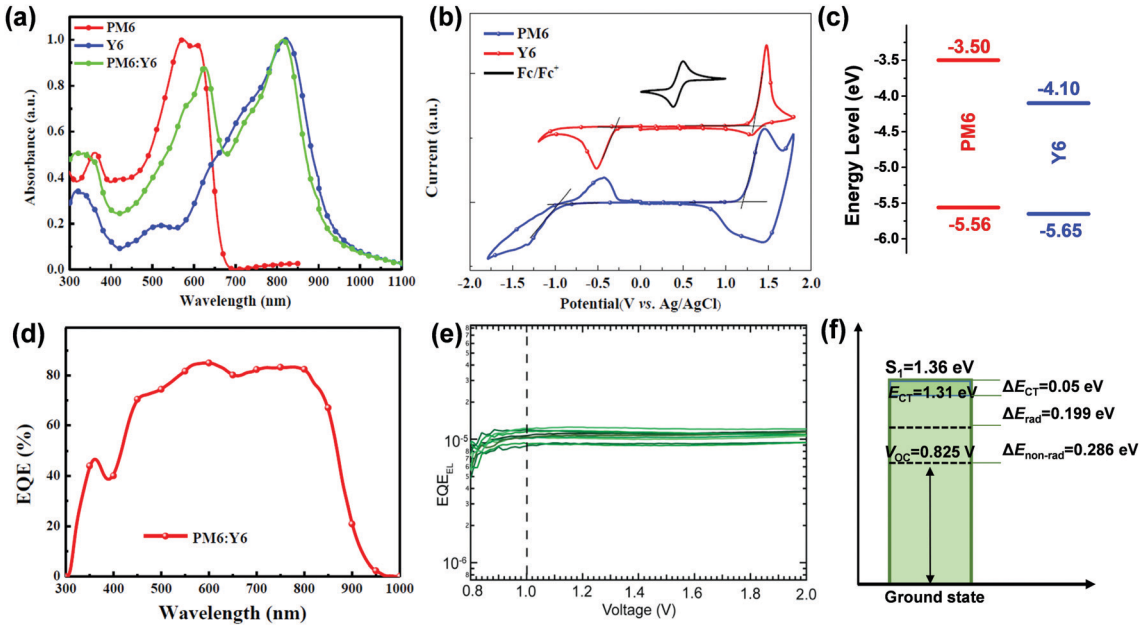

Fig. 2 (a) UV-vis absorption spectra of PM6, Y6 and the PM6:Y6-based blend films; (b) cyclic voltammetry (CV) plots and (c) energy levels of PM6 and Y6; (d) EQE curves of the PM6:Y6-based device;[34] Copyright 2019, Elsevier; (e) EQE_{EL} *versus* the applied bias for 12 devices based on PM6:Y6; and (f) a schematic representation of the breakdown of energy losses from S_1 to V_{OC}.[65] Copyright 2019, Wiley-VCH.

It was supposed that CT state dissociation could be assisted by the electronic polarization effects of Y6. In PM6:Y6-based BHJ films, the polarization energies increase significantly from the interfaces to the pure regions, which compensate for the coulombic binding of the CT state, therefore enabling barrier-free dissociation of the CT states. In addition, Zhang *et al.* compared the electron and hole transfer channels of CS in the devices using transient absorption (TA) spectroscopy, and discussed a possible underlying mechanism.[75] When a photon is absorbed by Y6, the photoexcited local excitation (LE) state is separated into free polarons through the intra-moiety excited (i-EX) states due to the strong intermolecular interaction between the conjugation units and the different electron affinities in the dimer structure of Y6. However, when a photon is absorbed by PM6, the LE state is separated into free polarons *via* the interfacial CT state.

Accurate characterization of molecular structures in the melt state, aggregated state and thin films is required to better understand the structure–processing–property relationships.[76,77] Single-crystal analysis of photovoltaic materials provides an effective method to investigate the relationship between structure and property, such as intrinsic electronic coupling, charge transport properties.[78,79] As shown in Fig. 3a and b, the extended Y6 crystal exhibits continuous and regular three-dimensional (3D) structure, which contain three types of Y6 molecular dimer.[78,80] Therefore, there is both overlap between the end groups (Pairs 1 and 2) and between the cores (Pair 3) in the Y6 molecular packing structure, leading to much larger electronic coupling between two adjacent molecules. It is known that charge mobilities are strongly influenced by the electronic coupling,[81,82] hence, Y6 exhibits ambipolar charge transport properties, with electron and hole mobility values of 1.8×10^{-4} and 5.6×10^{-4} cm^2 V^{-1} s^{-1}, respectively. Notably, the distinctive π–π molecular packing of Y6 is also evident in the PM6:Y6-base blend film, proved from grazing incidence wide-angle X-ray scattering (GIWAXS) measurements and molecular dynamics simulations.[80] Besides this, Y6 exhibits large exciton coupling between adjacent molecules in the range of 44–57 meV, which indicates that the excitons are well delocalized and diffuse. These features are conducive to reducing exciton–vibration coupling and thus slowing down the non-radiative decay rate.[80] More crucially, the estimated distance (d_{e-h}) between the hole and electron at the donor/acceptor interface increases from 22 to 51 Å due to the electron delocalization of Y6, leading to reduced coulombic attraction, as shown in Fig. 3c. Hence, effective charge generation can be achieved, although the driving force for the exciton dissociation is small.

Next, the probability of charge collection (P_C) of 97.7% and 91.8% under short-circuit and maximum power conditions, respectively, indicate negligible geminate recombination.[65] Measurement of the light intensity-dependent short-circuit current density and open-circuit voltage combined with the quantitative analysis of capacitance imply moderate non-geminate recombination with negligible bulk/surface trap-assisted recombination and excellent charge extraction (the effective charge carrier lifetime τ_{rec} is significantly larger than the effective extraction time τ_{ex}) of PM6:Y6-based devices. In addition, the PM6:Y6-based blend exhibits high and balanced charge mobilities, where the electron and hole mobilities are calculated to be 5.9×10^{-4} and 2.0×10^{-4} cm^2 V^{-1} s^{-1}, respectively.[34] These results contribute towards remarkable J_{SC} and FF values.

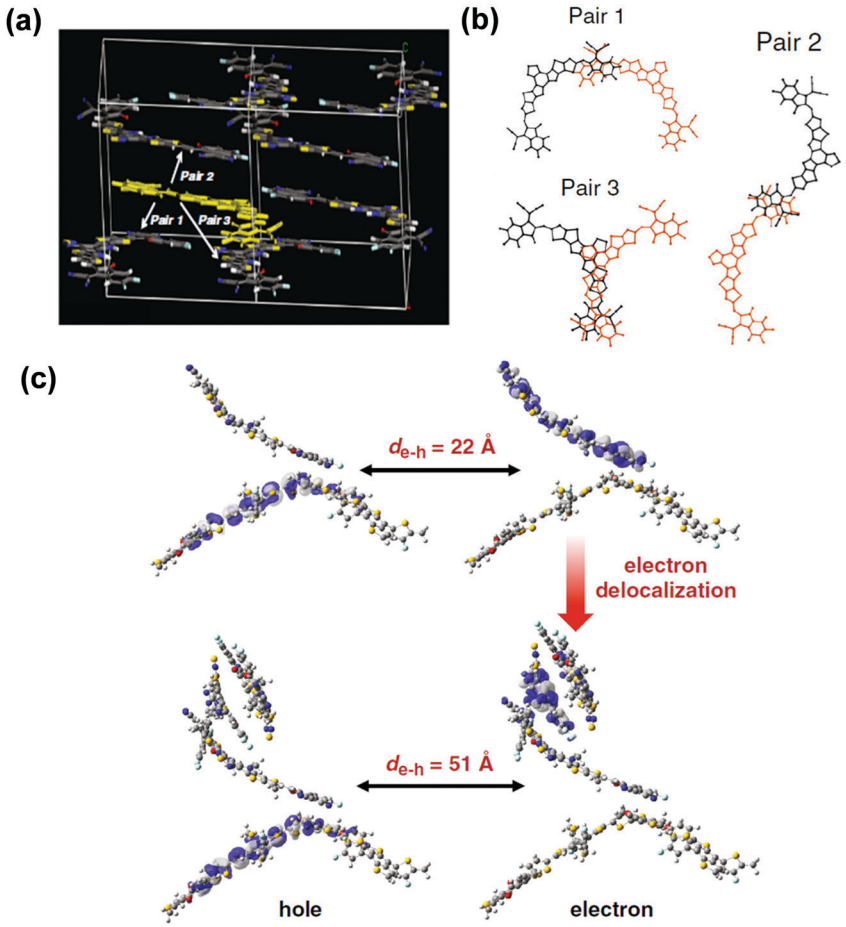

Fig. 3 (a) Molecular pairs in the Y6 single crystal. (b) Illustration of the molecular-dynamics simulations results for the packing in the pristine Y6. (c) Natural transition orbitals of the interfacial CT states using the TD-ωB97XD/6-31G(d,p) method coupled with the PCM model for molecular clusters (left: one PBDB-T-2F donor fragment with one Y6 molecule; right: one PBDB-T-2F donor fragment with three Y6 molecules).[80] Copyright 2020, Springer Nature.

3. Active layer optimization

3.1 Novel terpolymer based on PM6

Based on the rapid progress of NFAs, efficient polymer donors are desirable to construct high-performance OSCs. Among the various polymer donors, the design of terpolymer by incorporating a third monomeric unit into the copolymer backbone in a proper ratio has been proven to be a rational and facile strategy to precisely regulate the absorption spectra, energy level, aggregation and orientation of the original copolymers.[48,51,83–85] Depending on the third component, terpolymers can be classified into two types: (i) two donors and one acceptor monomer and (ii) two acceptors and one donor monomer. Herein, a series of terpolymers based on PM6 with excellent photovoltaic performance are highlighted, as shown in Fig. 4. Chemical structures of the typical terpolymer are shown in Fig. 5 and the corresponding properties and photovoltaic parameters are summarized in Table 1.

Increasing the withdrawing properties of the acceptor building block of polymer donors can lower the HOMO energy levels of the donors, therefore contributing towards improved V_{OC} values of

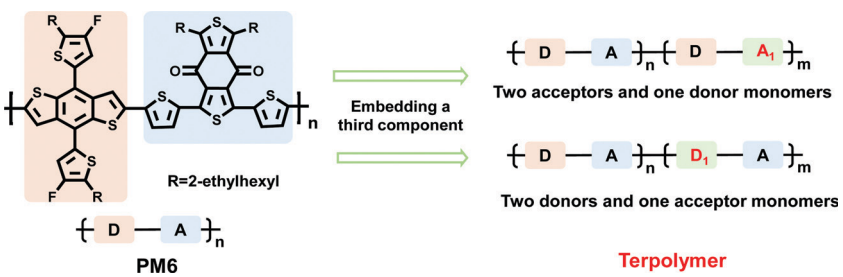

Fig. 4 Simplified schematic diagram for the classification of terpolymers.

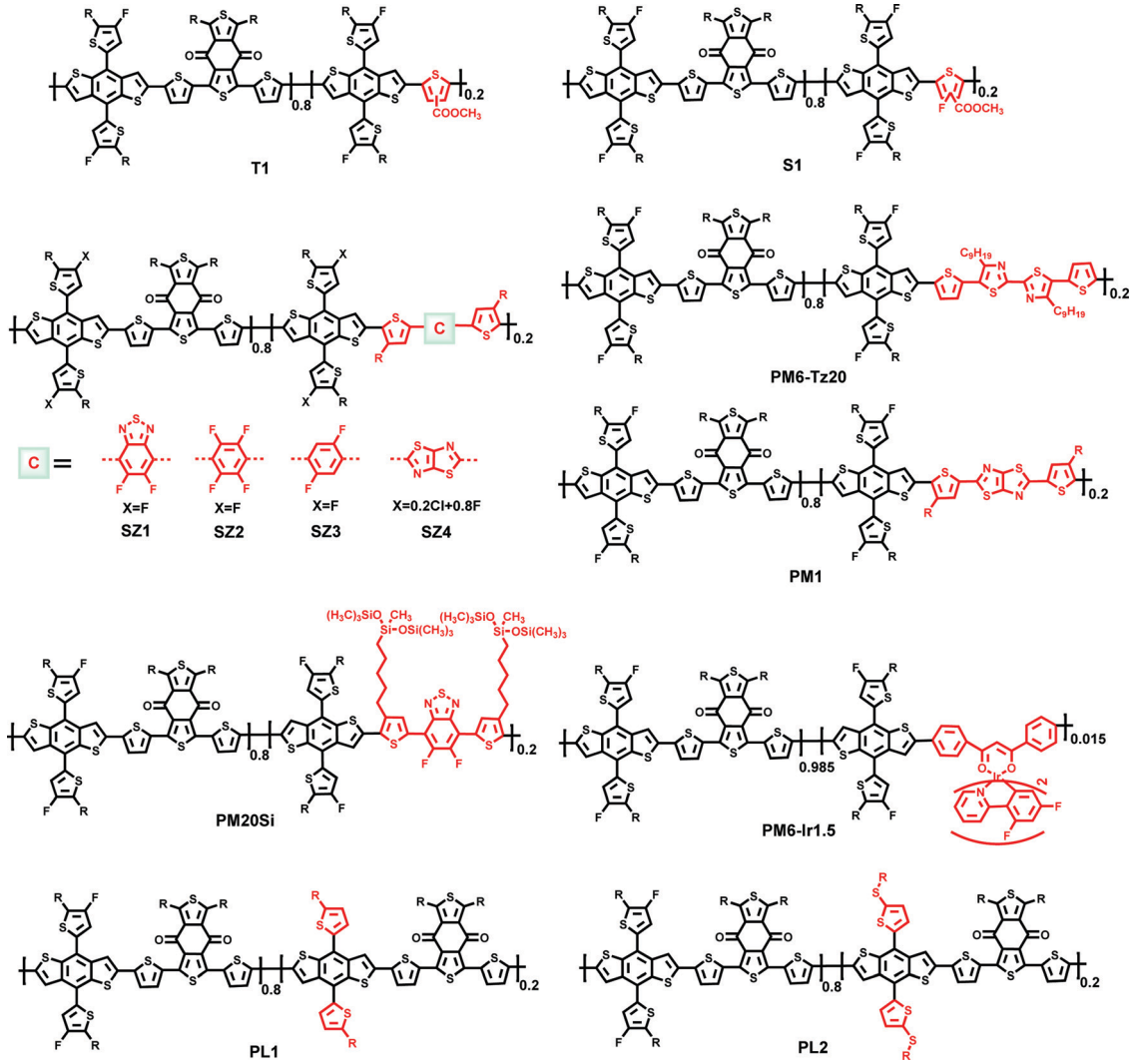

Fig. 5 Examples of the chemical structure of terpolymers (R = 2-ethylhexyl).

OSCs. Hou *et al.* introduced 20% of strong electron-withdrawing ester group-substituted thiophene (EST) into the PM6 polymer backbone and developed a novel terpolymer, T1, with lower HOMO levels, broader optical absorption and better solubility.[86] Combined with BTP-4F-12 (flexible alkyl chains modification of Y6), the devices with tetrahydrofuran (THF) as a processing solvent yielded a PCE of 16.1%. Besides EST, the electron-withdrawing fluorine atom (F) is another feasible choice for lowering the energy levels. In addition, a T1:BTP-4F-12-based device with an area of 1.07 cm^2 was fabricated *via* the blade-coating method using THF as the processing solvent, and an impressive PCE of 14.4% was achieved. Guo *et al.* overcame synthetic challenges and synthesized a novel building block (FE-T) based on a thiophene unit with the simultaneous substitution of EST and F.[87] Then, a novel terpolymer, S1, with a deeper HOMO level was developed by introducing 20% of FE-T into PM6. Besides this, benefiting from the S–O and S–F noncovalent interactions between FE-T and the adjacent thiophene, S1 exhibited reduced dihedral angles, which led to extended π-electron delocalization. Hence, compared with PM6, S1 shows more optimized crystallization and aggregation behavior, leading to enhanced face-on orientation and improved π–π stacking. Therefore, S1:Y6-based OSCs exhibit a remarkable PCE of 16.4%, with a significantly improved V_{OC} value of 0.877 V, J_{SC} value of 25.402 mA cm^{-2} and FF value of 73.7%, which are higher values than those of the PM6:Y6-based device (15.4% with a V_{OC} value of 0.839 V).

Reducing the HOMO energy of the donor and minimizing the energy offset between the donor and acceptor are effective in decreasing the energy loss for OSCs and achieving high V_{OC} values. While, reversely aligned energy levels between the donor and acceptor limit the effective charge separation. Optimizing the energy match between the donor and acceptor is critical to overcoming the trade-off. Yan *et al.* reported a series of terpolymer donors with a range of energy levels to find an optimal balance between efficient charge transfer and V_{OC}.[88] These novel polymers were synthesized by inserting around 20% of the third acceptor (difluorobenzo[*c*][1,2,5]thiadiazole (DFBT), *p*-difluorobenzene (DFB), tetrafluorobenzene (TFB), and thiazolo[5,4-*d*]thiazole (TzTz)) into the backbone of PM6/PM7.

Table 1 Summary of the optical, electrochemical performance and photovoltaic parameters of the corresponding terpolymers

Terpolymer	λ_{max} (nm)	E_g^{opt} (eV)	HOMO (eV)	LUMO (eV)	V_{OC} (V)	J_{SC} (mA cm^{-2})	FF (%)	PCE (%)	Ref.
T1[a]	—	1.82	−5.45	−3.64	0.853	25.2	75	16.1	86
S1	—	—	−5.52	−3.72	0.877	25.402	73.7	16.4	87
SZ1[b]	577	1.80	−5.50	−2.85	0.832	25.2	76.6	16.1	88
SZ2[b]	567	1.83	−5.51	−2.95	0.847	25.4	76.7	16.5	88
SZ3[b]	568	1.85	−5.44	−2.85	0.839	25.6	77.7	16.7	88
SZ4[b]	569	1.86	−5.51	−2.85	0.848	26.0	77.4	17.1	88
PM6-Tz20	—	1.84	−5.47	−3.59	0.85	26.3	77	17.1	89
PM1	—	—	−5.52	−3.59	0.87	25.9	78	17.6	90
PM20Si	607	1.81	−5.49	−3.07	0.80	26.92	70.44	15.2	91
PM6-Ir1.5[c]	—	—	−5.55	−3.62	0.839	26.09	77.98	17.1	92
PL1	620	1.84	−5.47	−3.52	0.82	25.57	78.1	16.4	93
PL2	620	1.84	−5.48	−3.53	0.81	24.63	75.5	15.1	93

[a] BTP-4F-12 served as an acceptor. [b] N3 served as an acceptor. [c] Y6-2 served as an acceptor.

These terpolymers possess fine-tuned energy levels, leading to higher V_{OC} values and better efficiencies. As a result, when blended with derivatives of Y6 (N3), all of these terpolymer-based devices exhibit impressive PCEs of over 16.1%. In particular, SZ4 matched N3 the best among these terpolymers, therefore leading to a PCE value of as high as 17.1%.

Apart from increasing the V_{OC} and J_{SC} values by tuning the energy levels of the donor, optimizing the molecular packing and orientation *via* a terpolymerization strategy also plays an important role in boosting the FF value, which is beneficial for effective charge generation, transport, and extraction, resulting in an improved PCE. In order to finely regulate the molecular packing to further optimize the morphologies of the corresponding active layer, Zhang *et al.* developed a novel terpolymer (PM6-Tz20) by incorporating 5,5′-dithienyl-2,2′-bithiazole (DTBTz, 20 mol%) as the third unit into the PM6 molecular backbone.[89] Combined with Y6, the M6-Tz20-based active layer shows optimized morphology with enhanced molecular packing, proper phase separation and high phase purity. These lead to the high-efficiency physical processes of the corresponding devices, including higher exciton dissociation and charge extraction efficiency, less charge recombination, higher and more balanced charge mobilities and increased PL quenching efficiencies. As a result, the PM6-Tz20:Y6-based OSCs achieved a noteworthy PCE of 17.1% with a significantly increased FF value of 0.77, while PM6:Y6-based devices only yielded a PCE of 15.7% with an FF value of 0.72. Meanwhile, Zhang *et al.* reported another high-performance terpolymer PM1 by incorporating 20% of thiophene–thiazolothiazole (TTz) into the PM6 backbone *via* random terpolymerization.[90] Based on the high crystallinity and charge mobility of PM1, the PM1:Y6-based blend showed favorable phase separation and good molecular aggregation. Therefore, a high PCE of 17.6% with a high FF value of 0.78 was achieved for the PM1:Y6-based OSCs.

Side chain modification is also an effective strategy by which to adjust the solubility, molecular packing and film morphology. Tan *et al.* synthesized a series of PM6-based terpolymers (PM10Si, PM20Si, and PM30Si), containing different siloxane-substituted (4,7-di(thiophen-2-yl)benzo[*c*][1,2,5]thiadiazole) (DTBT) content.[91] Compared with PM6, these terpolymer-based blends showed more favorable morphology when combined with Y6, leading to increased mobilities. As a result, the PM20Si:Y6-based device yielded a higher PCE with enhanced J_{SC} value.

Recently, Min *et al.* introduced a heavy metal containing component (1.5 mol% Ir complexes) into the PM6 backbone and synthesized a new terpolymer donor (PM6-Ir1.5) that shows increased steric hindrance and reduced aggregation tendency.[92] Blended with Y6-C2, a PM6-Ir1.5-based active layer exhibited suitable phase separation, contributing towards enhanced exciton dissociation and balanced charge transport. Hence, optimized PM6-Ir1.5:Y6-C2-based OSCs achieved high PCEs of up to 17.1%.

The PM6:Y6-based devices showed excellent efficiency. However, there are still factors that limit further improvements in PCE, such as efficient but sub-optimal hole transfer. Therefore, it is necessary to fine-tune the HOMO energy levels of donors to enable highly efficient hole transfer without severely sacrificing the V_{OC} value. Yan *et al.* developed two terpolymers, PL-1 and PL-2, *via* terpolymerization.[93] Compared with PM6, both terpolymers exhibited slightly upshifted HOMO energy levels and a slightly higher order of molecular packing. When blended with acceptor Y6, the blend films based on terpolymers showed a similar morphology to PM6-based blends. As a result, the OSCs based on PL-1:Y6 performed much better in terms of PCE (16.4%), with improved J_{SC} and FF values and a slightly decreased V_{OC} value than those based on PM6:Y6 (15.9%).

3.2 Ternary and quaternary OSC based PM6:Y6

In order to further improve the efficiency of OSCs, ternary devices with multiple donor or acceptor materials in the active layer are believed to be a promising strategy. Generally, ternary OSCs can be divided into four models according to the systems reported to date: charge transfer, energy transfer, parallel-like and alloy models. The incorporation of the third component provides one/multiple synergetic benefits to devices: (a) enabling complementary absorption with host materials to improve the J_{SC} value, (b) tuning the energy levels to enhance the V_{OC} value, (c) optimizing the morphology of the active layer, leading to favorable performances such as high-efficiency exciton dissociation, charge transport and collection, and suppressive recombination, hence contributing towards the enhancement in the J_{SC} and FF values.

3.2.1 Two donors and one acceptor as the ternary OSC active layer. The third component serving as a donor in the ternary OSCs is desirable to lead to a deeper HOMO energy level and proper crystallinity to achieve a higher V_{OC} value and optimized morphology of the active layer. Small molecule donors (SMDs) with diversified molecular structures can be used to easily tune the energy levels and optimize absorption. In addition, compared with polymers, SMDs generally exhibit better crystallinity, with the ability to regulate the morphology of ternary OSCs. Bao *et al.* reported a highly crystalline SMD (DRTB-T-C4, as shown in Fig. 7), serving as the third component in a binary device based on PM6:Y6.[94] DRTB-T-C4 with an appropriate coherence length of π–π stacking can prevent self-aggregation, facilitate a highly ordered structure and optimized morphology, leading to increased hole and electron mobilities (μ_h and μ_e), with a balanced μ_h/μ_e ratio of 1.01. As a result, an excellent FF value of as high as 0.813 can be achieved, therefore contributing towards an impressive PCE of 17.1% for PM6:DRTB-T-C4:Y6-based ternary OSCs. Li *et al.* demonstrated nematic liquid-crystalline benzodithiophene terthiophene rhodamine (BTR) with a similar structure and different crystallinity compared to that those of PM6, which simultaneously significantly enhanced the stacking and reduced the phase separation scale of the ternary active layer.[95] Hence, the introduction of BTR facilitated effective exciton dissociation, charge transport and collection, resulting in an improvement in the PCE from 15.7% for a PM6:Y6-based binary device to 16.6% for a BTR-incorporating ternary device. Similarly, Li *et al.* introduced BPR-SCl with a deep-lying HOMO and good crystallinity into PM6:Y6-based devices.[96] Simultaneously increased V_{OC}, J_{SC} and FF values were achieved for the ternary devices, with a high PCE of 16.7%. Zou *et al.* designed a novel donor ECTBD with the same central unit as PM6.[97] The introduction of ECTBD optimized the morphology of the ternary blend, resulting in increased J_{SC} and FF values. And then, the PM6:ECTBD:Y6-based ternary OSCs yielded a high PCE of 16.5%. Moreover, Peng *et al.* constructed ternary OSCs by introducing SMD (SM1) into PM6:Y6-based devices.[98] The similar structure ensured good compatibility between SM1 and PM6, and the highly-ordered stacking of SM1 optimized the morphology of the ternary blend, leading to improved J_{SC} and FF values, which were attributed to the improved charge extraction and exciton dissociation efficiencies, and reduced bimolecular recombination. And then, a high PCE of 16.6% was achieved for the ternary OSCs.

In addition to SMD, polymer donor materials have also been used as a third component to construct ternary OSCs. An *et al.* designed ternary OSCs by introducing a polymer donor S3 into the blend of PM6:Y6.[99] Motivated by the good compatibility, the two donors preferred to form an alloy-like state, leading to a well-developed morphology in the ternary active layer, which is beneficial to achieving enhanced charge generation and extraction, resulting in a highly improved FF value. Complementary absorption spectra of the two donors, as well as the deeper HOMO energy level of S3 contributed to simultaneously enhanced J_{SC} and V_{OC} values. As a result, the optimized ternary OSCs achieved a PCE of 17.5% with an FF value of 79.17%. Analogously, Zhang *et al.* constructed high-performance ternary OSCs by incorporating J71 into binary OSCs.[100] The resulting ternary devices showed a PCE of 16.5%, as a result of the complementary absorption, fine tuning of the energy levels, optimized molecular aggregation and phase separation. Recently, Guo *et al.* fabricated ternary OSCs consisting of PM6 and P1 as donors and Y6 as an acceptor.[101] Benefiting from the extended absorption, cascade-like energy levels and favorable morphology in the ternary blend, the optimized ternary OSCs achieved a PCE of 16.2%, with a significantly increased V_{OC} value and lower non-radiative recombination loss. Zhan *et al.* applied PBDB-T-SF as the third component into a PM6:Y6 system, in which the two had identical backbone structures with different side-chain orientation.[102] The loading of PBDB-T-SF tuned the polymer phase morphology *via* mesoscale interpenetrating polymer crowding, resulting in improved μ_h and balanced μ_h and μ_e values, as well as faster charge extraction and reduced trap-assisted recombination. Consequently, an improved efficiency of 16.4% with increased J_{SC} and FF values was achieved. Moreover, polymers with asymmetric blocks can also be used to optimize the photovoltaic performance of devices when introduced into binary systems as a third component. Yang *et al.* designed two asymmetrical polymers, PDHP-Th and PDHP-Ph, and introduced them into OSCs based on PM6:Y6 hosts.[103] The twisted backbone of the guest donors induced blue-shifted absorption spectra compared to that of PM6, which helped to improve the light harvesting. The finely mixed morphology of PDHP-Th with the host blend balanced the crystallinity of the donor and acceptor, leading to balanced charge mobility. As a result, ternary OSCs based on the PDHP-Th guest gave a PCE of 16.8%. And recently, Chen *et al.* employed a polymer donor, TPD-3F, as the third components into PM6:Y6-based devices.[104] The interaction parameter between PM6 and TPD-3F was extremely low, indicating good miscibility, which contributed towards the formation of a mixed phase. GIWAXS patterns indicated that the TPD-3F:Y6-based blend was more inclined to face-on orientation compared with the PM6:Y6 blend. Besides this, chloronaphthalene (CN) with a high boiling point, promoted a higher degree of π-stacking with proper phase separation. The various morphologies of the blends are summarized in Fig. 6. The optimized morphologies of the ternary devices exhibited efficient exciton dissociation and carrier transport, resulting in a significantly enhanced PCE of 17.0%.

3.2.2 Two acceptors and one donor as the ternary OSC active layer. Apart from introducing a donor as the third component, acceptor guests also play an important role in optimizing the performance of ternary OSCs. To this aim, Fullerene as the first available guest material has attracted wide studies in constructing ternary OSCs. Hou *et al.* introduced phenyl-C_{61}-butyric-acid–methyl ester ($PC_{61}BM$) into a PM6:Y6-based device and fabricated the ternary OSCs, which delivered an impressive PCE of 16.5%, with simultaneously improved V_{OC}, J_{SC} and FF values.[105] The improvement in the PCE for the ternary devices could be ascribed to the following reasons. First, the incorporation of $PC_{61}BM$ helped to increase the μ_e value, leading

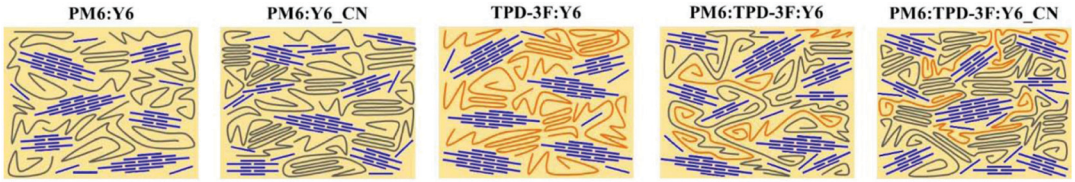

Fig. 6 Schematic representations of the morphologies in the various blend films.[104] Copyright 2020, American Chemical Society.

to a balance between the μ_h and μ_e values. Then, the $PC_{61}BM$ dispersed the aggregation of Y6 and enhanced the EQE_{EL}, which resulted in reduced nonradiative energy losses. Zhan *et al.* fabricated a ternary device by adding a small amount of phenyl-C_{71}-butyric-acid–methyl ester ($PC_{71}BM$) into a PM6:Y6-based device. The use of $PC_{71}BM$ increased the V_{OC} and J_{SC} values due to the higher LUMO energy (−3.90 eV) compared to that of Y6 (−4.15 eV) and relatively strong absorption in the region of 300–700 nm, which helped to achieve complementary absorption with the host material.[106] Besides this, the good compatibility between $PC_{71}BM$ and Y6 ensured that the main morphology of the host blend was unchanged and helped to improve the phase purity, contributing towards increased μ_h and μ_e values, as well as suppressive monomolecular recombination. Therefore, the V_{OC}, J_{SC} and FF values were simultaneously improved, resulting in a 7.7% enhancement in the PCE (16.7% *vs.* 15.5%) of the ternary OSC relative to that of the binary OSC. Ge *et al.* also introduced $PC_{71}BM$ into a PM6:Y6-based blend and developed ternary OSCs with a high PCE of 16.7%.[107] Notably, PM6:Y6:$PC_{71}BM$-based flexible ternary OSCs prepared on a PET substrate showed an excellent PCE of over 14%. Recently, Bu *et al.* made PM6:Y6-based binary and PM6:Y6:$PC_{71}BM$-based ternary devices to study the influence of vertical miscibility on the photovoltaic performance.[108] As reported, good vertical miscibility prevented charge traps and provided effective charge transport pathways. The PM6:Y6-base blend showed a uniform distribution of components in the vertical direction. While, the addition of $PC_{71}BM$ further optimized the uniform distribution of the components with improved content of Y6 on the top of the active layer, indicating more balanced charge transport, effective exciton dissociation, negligible bimolecular recombination and reduced trap-assisted recombination. As a result, an excellent PCE of 17.1% with a low sensitivity to film thickness for the PM6:Y6:$PC_{71}BM$ ternary OSCs was achieved. Yip *et al.* added 20% weight content of $PC_{71}BM$ into a PM6:Y6-based system and revealed that the addition of $PC_{71}BM$ had little effect on the packing of Y6, according to GIWAXS measurements.[80] And, the enhanced PCE (16.5%) of the ternary devices was mainly attributed to the improved charge transport properties.

NFAs with tunable absorption spectra, energy levels and molecular aggregation have also been widely used as the third component in ternary OSCs. Chen *et al.* synthesized two asymmetric NFAs (BTP-S1 and BTP-S2), as shown in Fig. 9, based on the same backbone as Y6 and two different end groups.[109] The PM6:BTP-S2-based device gave an outstanding EQE_{EL} of 2.3×10^{-2}%, which was one order of magnitude higher than that of the PM6:Y6 system (4.4×10^{-3}%), resulting in significantly lower nonradiative loss. Combining the high V_{OC} value of the BTP-S2-based device and high J_{SC} value of the Y6-based device, a ternary device was fabricated based on PM6:Y6:BTP-S2 to further improve the efficiency. Notably, when the BTP-S2 ratio changed from 10% to 50% in the acceptor mixture, efficiencies of over 17% could be achieved for all of the ternary OSCs. The champion PCE was as high as 17.4% for the ternary device with 20% BTP-S2, which showed highly improved V_{OC} and J_{SC} values. Introducing an NFA guest with red absorption and high LUMO energy levels also effectively induced the improvement in the V_{OC} and J_{SC} values of the ternary OSCs. Tang *et al.* introduced a NFA named SY3 as the third component in a PM6:Y6 host.[110] Due to the slightly red-shifted absorption and higher energy levels relative to those of Y6, the optimized ternary device realized an outstanding PCE of 17.1%, which was ascribed to the enhanced V_{OC} and J_{SC} values. Considering the morphology of NFA-guest ternary OSCs, Chen *et al.* developed a novel small acceptor BTP-M, which showed higher energy levels and lower crystallinity than Y6.[111] And then, ternary OSCs based on PM6:Y6:BTP-M were fabricated, where an alloy-like composite was formed between Y6 and BTP-M. Hence, the energy levels and morphology of the ternary active layer were optimized, leading to enhanced V_{OC} and J_{SC} values. Therefore, the optimized ternary device yielded an outstanding PCE of as high as 17.0%. Sun *et al.* designed two 3TP3T-4F and 3TP3T-IC NFAs, and incorporated as them as the third component in PM6:Y6-based binary OSCs.[112] 3TP3T-4F exhibited excellent compatibility with Y6, while poor compatibility was observed between 3TP3T-IC and Y6. Benefiting from the well-mixed acceptor phases (Y6 and 3TP3T-4F), the ternary device with a nondisrupted bicontinuous morphology delivered an improved PCE of 16.7%, higher than that of a 3TP3T-IC-based ternary device (15.6%), owing to a sacrificial morphology. Zhan *et al.* developed a new NFA IN-4F with a BDT central core, as a second acceptor to boost PM6:Y6-based device performance.[113] The optimized ternary device showed a high efficiency of 16.3%. This result indicated that the similarity in the structures of the host and guest acceptor helped to maintain the homogeneous fine film morphology of the corresponding binary active layer. At the same time, Zhan *et al.* incorporated IDIC into a PM6:Y6 blend to construct a ternary device with the well-maintained morphology of the host blend, and a PCE of 16.5% was achieved.[114] An *et al.* applied MF1 as a guest acceptor to generate an alloy model in a PM6:Y6-based host system, ascribed to the good compatibility of MF1 and Y6, which was proved by Raman mapping, contact angle and cyclic voltammetry measurements.[115] The ternary device achieved a high PCE of 17.2%, an over 8%

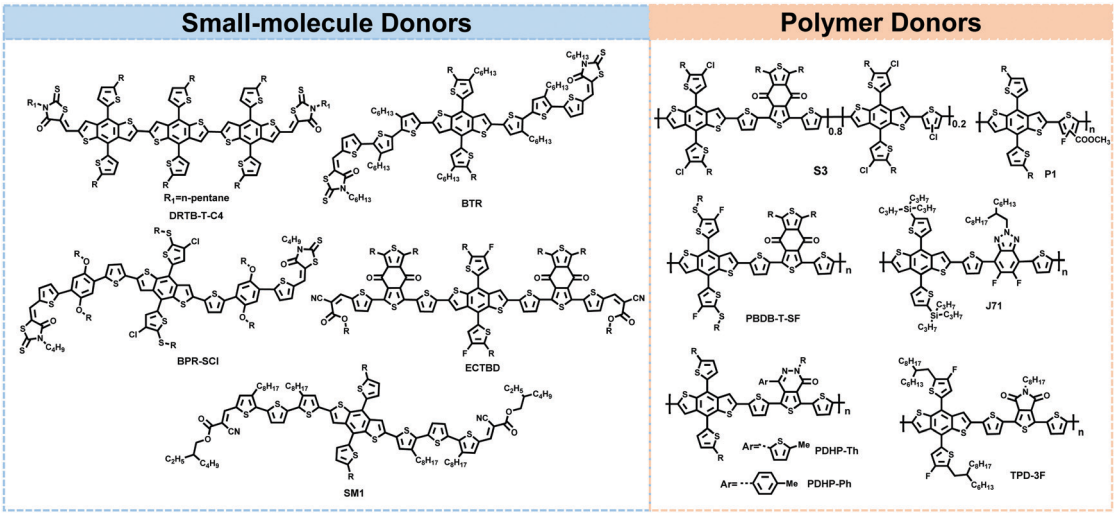

Fig. 7 Chemical structures of the third component (serving as a donor) in PM6:Y6-based ternary OSCs (R = 2-ethylhexyl).

improvement compared with the corresponding host device. Using the same ternary approach, this group also developed another ternary system by adding IT-4F into the PM6:Y6 blend and achieved a PCE of 16.3%.[116]

Different from the above, Liu *et al.* fabricated a series of ternary devices by incorporating acceptor guests with low miscibility and high LUMO energy levels into a PM6:Y6 system. The participation of a small amount of the third components enlarged the domain size and reduced the bimolecular recombination in the ternary blend, leading to enhanced J_{SC} and FF values.[117] As a result, the corresponding ternary OSCs based on PM6:Y6:ITCPTC, PM6:Y6:N7IT and PM6:Y6:PF2-DTC exhibited improved PCEs of 17.4%, 17.0 and 17.0%, respectively.

Gasparini *et al.* designed a novel small acceptor O-IDTBR and introduced it into a PM6:Y6 blend.[118] With the addition of O-IDTBR, the PCE of this ternary system increased from 15.2% to 16.6%. The increase in PCE can be attributed to better charge transfer and reduced trap-assisted recombination, where the O-IDTBR selectively mixed within the acceptor matrix and served as a charge relay. Notably, the ternary device exhibited

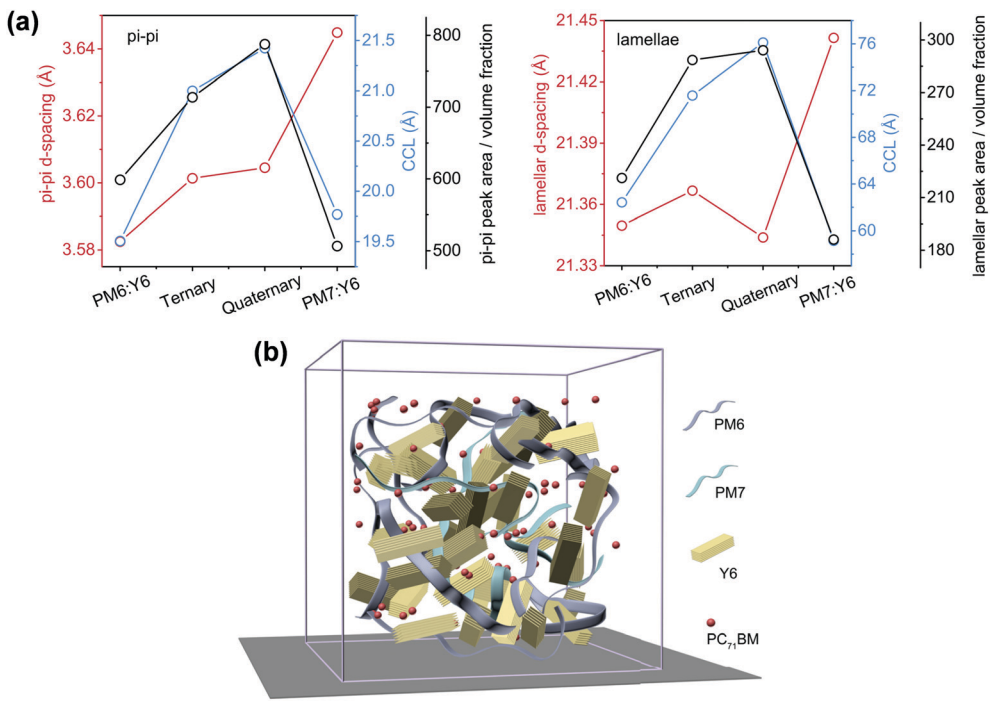

Fig. 8 (a) *D*-Spacing (red symbols), CCL (blue symbols) and peak area/volume fraction (black symbols) of π–π and lamellae diffraction peaks for blended films with different compositions. (b) Sketch of the arrangement of molecules in the quaternary blended films.[127] Copyright 2021, Springer Nature.

improved photostability, with a negligible PCE drop upon 1 sun illumination stress using a metal halide lap after 225 h, corresponding to minimized trap formation in the ternary devices.

Besides these above reports that applied A–D–A (or A–DA′D–A)-type acceptors as the third component, Cai *et al.* mixed a mid-band-gap star-shaped acceptor, FBTIC, with a PM6:Y6 blend and achieved a high PCE of 16.7% for the corresponding ternary device.[119] FBTIC provided complementary absorption to the host blend, with a high-lying LUMO energy level, contributing towards higher J_{SC} and V_{OC} values. In addition, according to single-crystal analysis, the star-shaped structure of FBTIC led to a complex 3D conjugated framework, benefiting charge transfer, and therefore leading to an improved FF value. Moreover, Zhang *et al.* designed ternary OSCs by introducing a commercially available polymer acceptor N2200 as the guest component into a PM6:Y6 blend.[120] The addition of N2200 suppressed the aggregation of Y6, leading to more favorable morphology with an appropriate domain size. Therefore, high photovoltaic efficiencies of 16.0% and 16.6% were obtained for blade-coated and spin-coated ternary OSCs, respectively.

3.2.3 Other ternary and quaternary OSCs. Up to now, the commonly used guest components in the ternary OSCs have been limited to relatively complex molecules. On the contrary, Zheng *et al.* constructed high-performance ternary OSCs by introducing a simple small molecule, BTF.[121] The addition of BTF led to an outstanding PCE of 16.5% for the optimized ternary device, with simultaneously improved V_{OC}, J_{SC} and FF values. Recently, Liao *et al.* introduced a liquid crystal small molecule (LCSM) named DFBT-TT6 into the PM6:Y6 system and constructed ternary OSCs to explore the influence of liquid crystal properties on the performance of devices.[122] Due to the good compatibility of DFBT-TT6 with PM6 and Y6, it was proved that DFBT-TT6 is mainly located at the D/A interface, contributing towards effective charge transfer and optimized morphology. Therefore, a significantly improved PCE of 17.1% was obtained for ternary OSCs compared with that of binary OSCs (15.8%). Tao *et al.* employed hydrogen bonding interactions between the guest component DIBC and host acceptor Y6 to regulate the crystallization, stacking and aggregation of acceptor, as well as optimize the morphology of the ternary blend.[123] OSCs based on the PM6:Y6:DIBC blend exhibited an improved PCE (16.4%) compared with the binary device (15.0%), with a significant improvement in the FF value from 71.28% to 77.12%. In addition, in order to suppress the recombination of excitons located in the CT state, Lin *et al.*

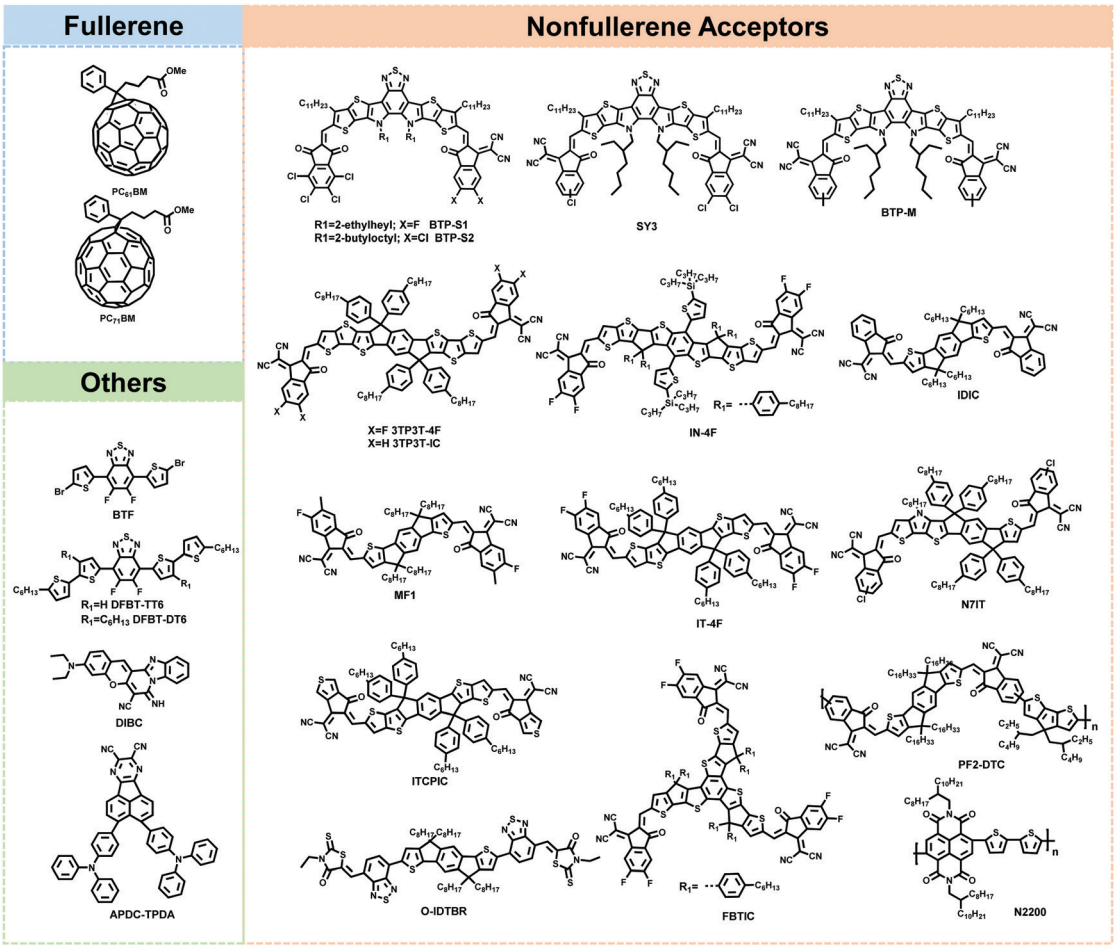

Fig. 9 Chemical structures of the third component (serving as an acceptor) in PM6:Y6-based ternary OSCs (R = 2-ethylhexyl).

Table 2 Photovoltaic parameters of the PM6:Y6-based ternary or quaternary OSCs

Active layer	Ratio (w/w)	V_{OC} (V)	J_{SC} (mA cm^{-2})	FF (%)	PCE (%)	Ref.
PM6 : DRTB-T-C4 : Y6	0.9 : 0.1 : 1.2	0.84	24.79	81.3	17.1	94
PM6 : BTR : Y6	0.95 : 0.05 : 1.2	0.839	25.8	76.7	16.6	95
PM6 : BPR-SCl : Y6	0.75 : 0.25 : 1	0.87	25.77	75	16.7	96
PM6 : ECTBD : Y6	0.85 : 0.15 : 1.2	0.848	25.54	76.24	16.5	97
PM6 : SM1 : Y6	0.85 : 0.15 : 1.2	0.831	25.7	77.5	16.6	98
PM6 : S3 : Y6	0.8 : 0.2 : 1.2	0.856	25.86	79.17	17.5	99
PM6 : J71 : Y6	0.9 : 0.1 : 1.2	0.85	25.55	76.0	16.5	100
PM6 : P1 : Y6	0.6 : 0.4 : 1.2	0.87	25.45	73.23	16.2	101
PM6 : PBDB-T-SF : Y6	0.85 : 0.15 : 1.2	0.856	25.21	76.11	16.4	102
PM6 : : PDHP-Th : Y6	1 : 0.1 : 1.2	0.850	26.60	71.7	16.8	103
PM6 : PDHP-Ph : Y6	1 : 0.03 : 1.2	0.823	26.58	68.2	15.4	103
PM6 : TPD-3F : Y6	0.9 : 0.1 : 1.2	0.893	25.83	73.7	17.0	104
PM6 : Y6 : $PC_{61}BM$	1 : 1.2 : 0.2	0.845	25.4	77.0	16.5	105
PM6 : Y6 : $PC_{71}BM$	1 : 1.2 : 0.1	0.861	25.1	77.2	16.7	106
PM6 : Y6 : $PC_{71}BM$	1 : 1.0 : 0.2	0.850	25.70	76.35	16.7	107
PM6 : Y6 : $PC_{71}BM_{(flexible)}$	1 : 1.0 : 0.2	0.828	23.57	72.03	14.1	107
PM6 : Y6 : $PC_{71}BM$	1 : 1.0 : 0.2	0.85	27.5	73.1	17.1	108
PM6 : Y6 : $PC_{71}BM$	1 : 0.96 : 0.24	0.83	26.0	75.9	16.3	80
PM6 : Y6 : BTP-S2	1 : 0.96 : 0.24	0.880	26.20	75.80	17.4	109
PM6 : Y6 : SY3	1 : 1 : 0.2	0.855	25.51	78.2	17.1	110
PM6 : Y6 : BTP-M	1 : 0.96 : 0.24	0.875	26.56	73.46	17.0	111
PM6 : Y6 : 3TP3T-4F	1 : 1.02 : 0.18	0.85	26.1	75.4	16.7	112
PM6 : Y6 : 3TP3T-IC	1 : 1.02 : 0.18	0.86	25.2	71.6	15.6	112
PM6 : Y6 : IN-4F	1 : 1.2 : 0.1	0.85	25.7	74.5	16.3	113
PM6 : Y6 : IDIC	1 : 1 : 0.2	0.868	25.39	74.92	16.5	114
PM6 : Y6 : MF1	1 : 1.08 : 0.12	0.853	25.68	78.61	17.2	115
PM6 : Y6 : IT-4F	1 : 0.96 : 0.24	0.844	25.40	75.9	16.3	116
PM6 : Y6 : ITCPTC	1 : 1.14 : 0.06	0.861	25.674	78.8	17.4	117
PM6 : Y6 : N7IT	1 : 1.14 : 0.06	0.854	25.538	77.7	17.0	117
PM6 : Y6 : PF2-DTC	1 : 1.14 : 0.06	0.854	25.728	77.5	17.0	117
PM6 : Y6 : O-IDTBR	1 : 0.85 : 0.15	0.85	25.75	76	16.6	118
PM6 : Y6 : FBTIC	1 : 1.0 : 0.2	0.866	24.6	77.9	16.7	119
PM6 : Y6 : $N2200_{(spin)}$	1 : 1.2 : 0.12	0.83	26.3	76	16.6	120
PM6 : Y6 : $N2200_{(blade)}$	1 : 1.2 : 0.12	0.83	26.3	74	16.0	120
PM6 : Y6 : BTF	1 : 1.2 : 0.1	0.853	26.11	74.22	16.5	121
PM6 : Y6 : DFBT-TT6	1 : 1.2 : 0.066	0.845	26.56	76	17.1	122
PM6 : Y6 : DIBC	1 : 1.2 : 0.1	0.83	25.61	77.12	16.4	123
PM6 : Y6 : APDC-TPDA	1 : 1.2 : 0.1	0.84	25.98	77.5	17.0	124
PM6 : Y6 : Br-ITIC	1 : 1.08 : 0.12	0.854	25.5	75.1	16.4	125
PM6 : Y6 : Br-ITIC : $PC_{71}BM$	1 : 1.08 : 0.12 : 0.12	0.853	25.8	76.4	16.8	125
PM6 : Y6 : IDIC : $PC_{71}BM$	1 : 1.0 : 0.2 : 0.1	0.866	26.19	75.29	17.1	126
PM7 : PM7 : Y6 : $PC_{71}BM$	0.8 : 0.2 : 1.2 : 0.25	0.859	26.55	79.23	18.1	127

developed a novel ternary device by introducing a delayed fluorescence (DF) emitter (APDC-TPDA) into the PM6:Y6-based host blend. The incorporation of APDC-TPDA extended the exciton lifetime and prevented energy transfer from the CT to the T1 state, leading to effective exciton diffusion and dissociation.[124] As a result, the optimized ternary device based on APDC-TPDA yielded a high PCE of 17.0%, with a highly improved FF (77.50%) value compared to that of the binary device (PCE of 15.2% and FF value of 71.87%). Notably, the APDC-TPDA-containing ternary OSCs exhibited excellent storage stability with around 96% of the initial PCE after 55 days of storage under ambient conditions (temperature of 25 °C and relative humidity of 25%, room light).

Consistent with the effect of the ternary device, a quaternary strategy was adopted to further improve the efficiency of OSCs. Zhang *et al.* fabricated quaternary OSCs based on a PM6:Y6 host blend by incorporating Br-TICI and $PC_{71}BM$ as guest components.[125] Compared to the binary (PM6:Y6, PCE of 15.7%) and ternary (PM6:Y6:Br-ITIC and PM6:Y6:$PC_{71}BM$, PCEs of 16.4% and 16.2%, respectively) devices, the quaternary device presented a further improved efficiency of 16.8%. Subsequently, Zhan *et al.* prepared a quaternary device based on PM6:Y6:IDIC:$PC_{71}BM$ and achieved an excellent PCE of 17.1%.[126] Liu *et al.*[127] fabricated quaternary devices comprising PM6:Y6 host pairs with an additional donor PM7 and acceptor $PC_{71}BM$. PM7 has a similar structure to that of PM6 but with a deeper HOMO energy level and $PC_{71}BM$ exhibits higher LUMO energy levels than Y6, affording a cascading energy level alignment and resulting in longer exciton diffusion times. GIWAXS measurements showed that the quaternary blend showed the largest crystal coherence lengths (CCL) and peak area in both the π–π stacking and lamellar stacking directions. The results are summarized in Fig. 8a, which indicated the improved crystallinity and crystal quality of the quaternary blend. A schematic of the molecular packing in the quaternary blend is shown in Fig. 8b. The mixture of PM6 and PM7 contributes towards a fibrillar network, and optimized the packing of Y6 due to the different interaction of PM7 with Y6 compared with that of PM6. The addition of $PC_{71}BM$ was found not to disrupt the host morphology. As a result, the PM6:PM7:Y6:PC71BM-

based quaternary device yielded an outstanding PCE of over 18%. In addition, the quaternary device exhibited excellent photostability and storage stability. After 1000 h of illumination, the device maintained 81% of its initial PCE. And, after 1000 h of aging at an average temperature of 41.5 °C and relative humidity of 12.5%, the device retained 97.2% of its initial PCE (Table 2).

3.3 Various treatment procedures of the PM6:Y6 blend

Apart from optimizing the photovoltaic materials as demonstrated above, controlling the kinetics and thermodynamics during the evolution of the film formation, as well as grasping the thermal transition of molecules in the blend film to regulate the morphology of the active layer have also attracted considerable attention. Specifically, tuning the D/A ratio, solvent/solid additives processing, solvent selection, and thermal/solvent annealing are the widely used approach to optimize the active layer for solution-processed OSCs. Recently, Liu *et al.* revealed the relationship between the processing solvent and thermal annealing conditions, film morphology, and photovoltaic performance of a PM6:Y6-based device.[79] In the chloroform (CF) processed film, Y6 with a banana shape, adopted π–π stacking through its end group along the cube body diagonal with two Y6 molecules and formed 1D channel. And two 1D channels were integrated to form a polymer-like conjugate backbone with a 2D network. The two charge channels with special orientation improved the charge mobilities and current density. Furthermore, after thermal annealing, the π–π stacking became tighter and the crystal coherence length was increased, thus further improving the performance. As a result, the best optimized device delivered a PCE of as high as 16.9%. By contrast, the device processed in chlorobenzene (CB) only showed a PCE of 12.2% due to the small and discrete oriented crystallites of Y6. Subsequently, Ma *et al.* fabricated a series of devices using CB, 1,2,4-trimethylbenzene (TMB) and *ortho*-xylene (*o*-XY) as processing solvents *via* slot-die coating.[128] Interestingly, the devices with different solvents exhibited similar morphology through controlling the solution and substrate temperature, therefore yielding similar PCEs of 15.2%, 15.4% and 15.6% for CB, TMB and *o*-XY, respectively. These results indicated that similar aggregation states and kinetics processes during film formation result in the different solvent processed blends having similar morphologies. Tan *et al.* proposed a solvent-flushing strategy using acetylacetone (Acac, as shown in Fig. 10) to optimize the component distribution in the active layer for PM6:Y6-based OSCs.[129] Due to the partial solubility of Y6 and insolubility of PM6 in Acac, the acceptor on the surface of the flushed blend could be taken away, leading to an inhomogeneous vertical concentration distribution. Then, the inverted OSCs based on PM6:Y6 exhibited increased PCEs from 15.4% to 16.5%.

Different from the empirical trial-and-error approaches of processing thermal annealing, Ade *et al.* proposed a relatively rational annealing strategy named double-annealing method, involving aggregation transitions. Thermal transition of the acceptor Y6 (102 ± 1 °C) was evaluated using a UV-vis method.[130] And then, after double-annealing treatment under a low temperature of 100 °C first and a second higher temperature

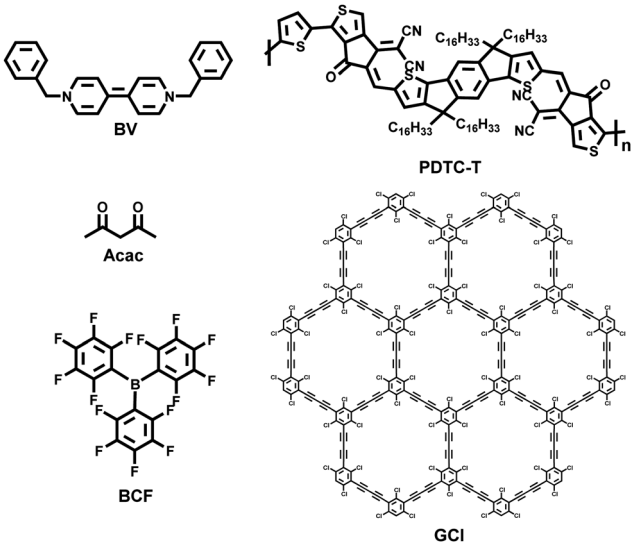

Fig. 10 Chemical structures of additives applied in a PM6:Y6-based system.

of 120 °C, the PM6:Y6:$PC_{71}BM$-based ternary OSCs achieved 16.8% efficiency, representing a 5% and 6% improvement compared with the device that was single-annealed at 100 and 120 °C, respectively.

Zhang *et al.* explored the *p*-dopant tris(pentafluorophenyl)-borane (BCF) for use in PM6:Y6-based OCSs.[131] Due to the electron-deficient B atoms in BCF, the dopant prefers to interact with PM6 and frustrated Lewis pairs, leading to enhanced π–π stacking, with the efficiency of the PM6:Y6 device increasing to 16.0% from 15.4%. Anthopoulos *et al.* demonstrated an n-type dopant BV and incorporated it in the PM6:Y6 and PM6:Y6:$PC_{71}BM$-based host blends, respectively.[132] The addition of BV results in increased optical absorption and optimized phase separation with improved molecular packing, contributing towards balanced charge transport. Hence, high efficiencies of 16.0% and 17.1% were achieved for BV-doped PM6:Y6 and PM6:Y6:$PC_{71}BM$-based devices, respectively. Moreover, Jiu *et al.* proposed chlorine-functionalized graphdiyne (GCl) as a novel solid additive applied in a PM6:Y6 system, resulting in the PCEs of the corresponding devices significantly improving to 17.3%, with simultaneously increased J_{SC} and FF values.[133] The high efficiency was attributed to the enhanced crystallinity and prominent phase separation, and hence more effective physical processes upon the addition of GCl. Likewise, Yang *et al.* introduced a new polymer acceptor (PIDTC-T) as the solid addition into a PM6:Y6-based device and achieved a remarkable PCE of 16.8%.[134] Shoaee *et al.* fabricated a thick device (~400 nm) based on PM6:Y6 using chloronaphthalene (CN) addition to regulate the packing and crystallinity of photovoltaic materials. And then, a PCE of 14.4% was achieved (Table 3).[135]

3.4 Interfacial engineering and electrode progress

Designing novel donor/acceptor materials and optimizing the morphology of the active layer are the key strategies to improve

Table 3 Photovoltaic parameters of PM6:Y6-based OSCs subjected to different treatment processing

Active layer	Processing conditions	V_{OC} (V)	J_{SC} (mA cm^{-2})	FF (%)	PCE (%)	Ref.
PM6:Y6	CB 80 °C	0.796	21.16	72.15	12.2	79
PM6:Y6	CF 80 °C	0.835	26.52	76.21	16.9	79
PM6:Y6	CB solution/substrate temperature (80/80 °C)	0.82	25.9	70.0	15.2	128
PM6:Y6	*o*-XY solution/substrate temperature (100/100 °C)	0.81	26.6	70.3	15.6	128
PM6:Y6	TMB solution/substrate temperature (110/110 °C)	0.80	26.4	70.9	15.4	128
PM6:Y6	Solvent-flushing (0.5% Acac)	0.857	25.50	75.57	16.5	129
PM6:Y6:$PC_{71}BM$	Single-annealed 100 °C	0.84	25.40	75	16.0	130
PM6:Y6:$PC_{71}BM$	Single-annealed 120 °C	0.83	25.90	74	15.9	130
PM6:Y6:$PC_{71}BM$	Double-annealed 100/120 °C	0.83	26.60	76	16.8	130
PM6:Y6	0.01 wt% BCF	0.84	25.96	73.47	16.0	131
PM6:Y6:$PC_{71}BM$	0.004 wt% BV	0.84	26.3	77	17.1	132
PM6:Y6	1 wt% GCl	0.840	26.09	79.05	17.3	133
PM6:Y6	2 wt% PIDTC-T	0.847	25.50	77.6	16.8	134
PM6:Y6	1.5% CN 400 nm	0.81	26.3	68.1	14.4	135

the efficiency of OSCs. Meanwhile, interfacial engineering and electrode modification also play important roles for effective charge transport and extraction, and subsequently result in high performance of OSCs with extensive characteristics such as flexibility, semitransparent, *etc.* Excellent conductivity, appropriate work function and surface energy are desirable for interfacial layer materials to ensure better energy alignment and interfacial contact. According to the different transporting characteristics, the interfacial layer can be divided into a hole transport layer (HTL) and electron transport layer (ETL), corresponding to hole transport materials (HTMs) and electron transport materials (ETMs), respectively.

Poly(3,4-ethylenedioxythiophene):poly(styrenesulfonate) (PEDOT:PSS) is one of the most widely used HTMs in OSCs due to its high transparency in the visible region and solution processability. However, some weaknesses such as modest conductivity and strong acidity limit the efficiency of the corresponding OSCs. A series of strategies have been investigated to optimize the performance of PEDOT:PSS. In aqueous solution, the hydrophilic and insulating PSS dominates the surface region of coiled/core–shell PEDOT:PSS, while hydrophobic and conductive PEDOT occupies the core region, leading to limited conductivity to achieve an efficient charge transport process. Therefore, Guo *et al.* dropped graphitic carbon nitride (g-C_3N_4) into PEDOT:PSS to break the shield of PSS and release more PEDOT, subsequently resulting in improved conductivity.[136] The PM6:Y6-based device with g-C_3N_4:PEDOT:PSS as a HTL exhibited an improved PCE of 16.4% with an enhanced FF and J_{SC} value, as a result of improved charge transport and suppressed charge recombination. Li *et al.* modified PEDOT:PSS by dropping dopamine hydrochloride (DA-HCl), where the dopant reacted with PSS and yielded PSS-DA, leading to the enhanced intermolecular stacking of HTM (PEDOT:PSS:DA).[137] Therefore, the PEDOT:PSS:DA exhibited enhanced work function and conductivity, contributing to a high PCE of 16.6% for corresponding OSCs based on PM6:Y6. Recently, Huang *et al.* introduced a series of novel oxoammonium salts ($TEMPO^+X^-$) to simultaneously optimize the work function and conductivity.[138] When using $TEMPO^+Br^-$ as a HTL, the device based on PM6:Y6 exhibited an improved PCE of 16.1%.

Regulating the surface-free energy (SFE) of PEDOT:PSS in conventional devices can effectively tune the vertical distribution of the donor and acceptor in the active layer, where the donor (acceptor) enriches near to the anode (cathode) regions. Alharbi *et al.* introduced Nafion to achieve chain separation between PEDOT and PSS, leading to the decreased SFE of PEDOT:PSS, due to the favorable enrichment of the donor.[139] By accurately tuning the ratio of Nafion, the PM6:Y6-based device with PEDOT:PSS–Nafion (4 : 1) as a HTL achieved a high PCE of 16.3%. Besides this, the "molecular lock" between HTMs and active layer materials also brings about vertical distribution, as well as mechanical contact. Sun *et al.* added chloroplatinic acid (CPA) into PEDOT:PSS and constructed a "molecular lock" with the polymer donor PM6, leading to a denser and more orderly stacking of PM6 near the surface of CPA dropped PEDOT:PSS.[140] Therefore, the PCEs of PM6:Y6-based OSCs with dropped PEDOT:PSS as a HTL attained 16.5%, with an enhanced FF values of 77%, as a result of reduced trap-assisted recombination and prolonged charge carrier lifetime. Wang *et al.* presented a bilayer structure HTL of copper(I) thiocyanate (CuSCN) and poly[(9,9-dioctylfluorenyl-2,7-diyl)-*alt*-(4,4′-(*N*-(4-butylphenyl))))] (TFB), where the TFB contributed towards tuning the work function of CuSCN and enhancing the interfacial contact between CuSCN and the active layer PM6:Y6.[141] As a result, a PCE of 15.1% was achieved for the corresponding device.

Apart from PEDOT:PSS, transition metal oxides such as V_2O_5, WO_3, *etc.* are other widely used HTMs. However, the key point of these HTMs is the high annealing temperature, which leads to complex device manufacturing. To address these issues, Anthopoulos *et al.* demonstrated liquid exfoliated 2D WS_2 nanosheets as a HTM, changing the work function of the indium tin oxide (ITO) without further treatment.[142] Owing to reduced bimolecular recombination, the OSCs comprising WS_2 as a HTL exhibited an excellent PCE with improved FF and J_{SC} values (PCE of 15.8%, FF of 73% for the PM6:Y6-based device and a PCE of 17.0% and FF of 78% for the PM6:Y6:$PC_{71}BM$-based device). Cho *et al.* reported another approach to achieving annealing-free processing for the HTL.[143] Different from anhydrous system processing *via* high-temperature annealing, a small amount of water contributes towards removing the acetylacetonate ligand of $MoO_x(acac)_2$ easily through hydrolysis. Hence, compared with MoO_x prepared *via* an anhydrous sol–gel method (7.7% without annealing), the PM6:Y6-based device with

aqueous sol–gel-prepared MoO_x yielded a significantly higher PCE of 17.0% without any annealing process.

Guo *et al.* introduced bismuth oxychloride (BiOCl) NPs as a HTM to produce a material with a high oxygen vacancy content, favorable interfacial contact, high chemical stability, and excellent optoelectronic properties, that does not require post treatment.[144] Compared with traditional PEDOT:PSS, an increase of 3% was achieved for PM6:Y6-based devices with BiOCl NPs serving as a HTL. Besides this, OSCs based on BiOCl displayed better stability attributed to the reduced chemical reactivity and hydrophobicity of BiOCl, which enabled a kinetic barrier for H_2O penetration. Kim *et al.* applied fluorine-functionalized reduced graphene oxide (FrGO) as a HTL *via* a spray coating method into a PM6:Y6-based device and achieved an efficiency of 13.3%.[145] Subsequently, Chen *et al.* reported a novel conjugated polyelectrolyte $PCPDTK_{0.50}H_{0.50}$-TT as a HTL, which meets the requirements of printing preparation.[146] The corresponding OSCs based on PM6:Y6:$PC_{71}BM$ achieved a PCE of 16.3%, with an area of 0.04 cm^2.

Wide-bandgap metal oxides also have been widely used in OSCs as ETLs, such as ZnO, V_2O_x, SnO_x, *etc.*, due to their high selectivity in extracting electrons. However, the trap states and localized electronic states caused by the oxygen vacancies of these metal oxides limit the high performance of their corresponding OSCs. In order to passivate the oxygen vacancies, Lin *et al.* introduced polar solvents such as alcohol-amines with Lewis basicity, which bond with oxygen vacancies on the ZnO surface, leading to a lower trap density and higher electron mobility.[147] As reported, when triethanolamine (TEA)-passivated ZnO was used as an ETL, the device based on PM6:Y6 exhibited an enhanced PCE of 15.6%, with an improved J_{SC} value. Interestingly, Xie *et al.* adopted perylene bisimide with benzenesulfonic acid (PBI-SO_3H) to optimize ZnO. The PBI-SO_3H not only enhanced the solubility of molecules in water but also facilitated the formation of ionic bonds between sulfonic acid and Zn atoms, contributing towards increased hole blocking ability and highly efficient electron collection and transportation in inverted OSCs.[148] As a result, an efficiency of up to 15.4% was achieved for a PM6:Y6-based device. Yang *et al.* spin-coated a thin film of potassium hydroxide (KOH) on a ZnO surface to obtain potassium ion (K^+) modified ZnO, which interacted with the acceptor in the active layer, resulting in a higher content of the acceptor near to the ZnO surface.[149] Benefiting from the optimized vertical morphology, the corresponding device based on PM6:Y6 exhibited an improved PCE of 15.7%.

Graphene has been reported to serve as a HTM due to its unique characteristics such as high carrier mobility, transparency, mechanical flexibility, and compatibility with solution processability, *etc.* In addition, it also functions as an ETM. Lv *et al.* dispersed graphene into (*N*,*N*-dimethyl-ammonium *N*-oxide)propyl perylene diimide (PDINO) and developed a novel n-doped ETM (PDINO-G), as verified by electron spin resonance (ESR), Raman spectroscopy and X-ray electron spectroscopy (XPS) measurements.[150] PDINO-G exhibited improved conductivity and charge extraction rate, and reduced charge recombination. When the n-doped PDINO-G was introduced as an ETL, the PM6:Y6-based device displayed an improved PCE of 16.5%. After that, this group reported 3D surfactant (POSSFN and ADMAFN)-dispersed graphene, wherein the amino groups in the surfactants interact with graphene.[151] Compared with 2D graphene, the 3D n-doped graphene exhibited prominent processability, faster charge carrier extraction, and reduced recombination. Hence, the PM6:Y6-based OSCs yielded 15.9% and 16.1% with POSSFN-G and ADMAFN-G as ETMs, respectively.

Hu *et al.* synthesized a type of n-doped conjugated polyelectrolyte (CPEs, PFBP-Br and PFBP-I) *via* an Aldol condensation protocol between bis-isatin and bis-oxindole monomers, which exhibited enhanced charge delocalization, higher doping levels and conductivity.[152] With PFBP-Br serving as an ETM, the device based on PM6:Y6 achieved a PCE of over 16%. Besides this, the devices showed insensitivity to PFBP-Br thickness, with PCEs of over 14% and 11% for 30 and 60 nm PFBP-Br, respectively, which are beneficial for the fabrication of large-area OSCs. In addition, Tan *et al.* fabricated a PM6:Y6-based device with printable SnO_2 as an ETL, yielding excellent efficiency.[153] When the thickness of SnO_2 increased from 10 to 160 nm, the corresponding PCEs showed a slight decrease from 16.1% to 13.1%. In addition, large-area OSCs of 100 mm^2 based on printed SnO_2 cathode interlayers achieved an excellent PCE of 12.7%. Subsequently, this group introduced aluminum(III) acetylacetonate ($Al(acac)_3$) as an ETL and constructed a semi-transparent OSC (ST-OSC) based on PM6:Y6, yielding a PCE of 12.4% with an average visible transmittance (AVT) of 25.33%.[154] Encouragingly, the corresponding large-area 100 mm^2 ST-OSC still achieved a high PCE of 11.3%.

Furthermore, Zhang *et al.* synthesized a small-molecule electrolyte (HDSID) and applied it in OSCs as an ETL, leading to 15.6% efficiency for a PM6:Y6-based device.[155] Xia *et al.* developed a novel reaction between metal-carbon triple bonds and a carbon–carbon triple and afforded a metallic-aromatic system with a d_π–p_π conjugated structure (Os$\equiv$C), which was found to be a good ETM with which to construct OSCs. The device based on PM6:Y6 demonstrated a high PCE of 16.3%.[156]

Apart from the interfacial layers, the electrodes play an important role in OSCs. Meanwhile, the selection of the electrodes is one of the key factors in fabricating ST-OSCs, which exhibit special applications, such as in windows, buildings, greenhouses, *etc.* Ade *et al.* introduced novel bimodal silver nanowires (AgNW-BM) containing two different aspect ratios (short/thick with a low aspect ratio and long/thin with a high aspect ratio).[157] As reported, the AgNW-BM exhibited reduced sheet resistance and high visible transmittance. Hence, the ST-OSCs based on PM6:Y6 with AgNW-BM as a top electrode (at the top of the device, used to extract charge) exhibited a high efficiency of 9.79%, with an AVT of 23%. Recently, Lu *et al.* employed Ag/ITO as an electrode to prepare ST-OSCs. By changing the thickness of Al and ITO, the transmittance of the devices was improved, with a high efficiency of 10.2% with AVT of 28.6% being realized for the PM6:Y6-based device.[158] An *et al.* replaced the Al electrode in opaque OSCs with 1 nm Au combined with different thicknesses of Ag to construct ST-OSCs.[159] The trade-off

Table 4 Photovoltaic parameters of PM6:Y6-based OSCs with different interfacial layers/electrodes

Active layer	Interfacial layer/electrode	V_{OC} (V)	J_{SC} (mA cm^{-2})	FF (%)	PCE (%)	Ref.
PM6:Y6	g-C_3N_4:PEDOT:PSS	0.84	26.71	73	16.4	136
PM6:Y6	PEDOT:PSS:DA	0.840	25.52	77.1	16.6	137
PM6:Y6	PEDOT:PSS(TEMPO$^+$Br$^-$)	0.82	27.18	72.59	16.1	138
PM6:Y6	PEDOT:PSS–Nafion (4 : 1)	0.84	25.76	75.40	16.3	139
PM6:Y6	CPA/PEDOT:PSS	0.84	25.5	77.0	16.5	140
PM6:Y6	CuSCN/TFB	0.85	24.45	72.69	15.1	141
PM6:Y6	WS_2	0.84	25.9	73	15.8	142
PM6:Y6:$PC_{71}BM$	WS_2	0.84	26.0	78	17.0	142
PM6:Y6	Aqueous MoO_x	0.843	27.53	73.8	17.0	143
PM6:Y6	BiOCl NPs	0.83	27.07	71.70	16.1	144
PM6:Y6	S-FrGO	0.77	24.64	69.9	13.3	145
PM6:Y6:$PC_{71}BM$ (0.04 cm^2)	$PCPDTK_{0.50}H_{0.50}$-TT	0.854	25.10	75.9	16.3	146
PM6:Y6:$PC_{71}BM$ (1.0 cm^2)	$PCPDTK_{0.50}H_{0.50}$-TT	0.872	17.33	67.5	10.2	146
PM6:Y6	TEA-capped ZnO	0.820	29.19	65.20	15.6	147
PM6:Y6	ZnO:PBI-SO_3H	0.84	24.67	73.46	15.4	148
PM6:Y6	ZnO/KOH	0.85	27.1	68.1	15.7	149
PM6:Y6	PDINO-G	0.85	25.65	75.78	16.5	150
PM6:Y6	POSSFN-G	0.849	25.34	73.93	15.9	151
PM6:Y6	ADMAFN-G	0.845	25.45	74.91	16.1	151
PM6:Y6	PFBP-Br	0.83	26.12	73.49	16.2	152
PM6:Y6	SnO_2 (10 nm)	0.831	26.63	72.75	16.1	153
PM6:Y6	SnO_2 (160 nm)	0.819	25.28	63.14	13.1	153
PM6:Y6	$Al(acac)_3$	0.817	20.71	73.34	12.4	154
PM6:Y6	HDSID	0.84	25.84	71.84	15.6	155
PM6:Y6	Os≡C (30)	0.87	25.21	74.19	16.3	156
$PM6:Y6_{(ST\text{-}OSCs)}$	AgNW-BM	0.716	20.84	61.26	9.12	157
$PM6:Y6:PC_{71}BM_{(ST\text{-}OSCs)}$	Ag/ITO	0.88	17.9	65.2	10.2	158
$PM6:Y6_{(ST\text{-}OSCs)}$	1 nm Au/10 nm Ag	0.852	20.35	71.36	12.3	159
$PM6:Y6_{(FST\text{-}OSCs)}$	D-PEDOT:PSS	0.80	19.28	68.36	10.5	160
$PM6:Y6_{(flexible)}$	Em-Ag/AGNWs:AZO-SG	0.832	25.05	72.97	15.2	161

between efficiency and transmittance could be balanced by adjusting the thickness of Ag. A PCE of 12.3% with an AVT of 18.6% was obtained for a PM6:Y6-based device using 10 nm Ag.

In addition, Ge *et al.* optimized PEDOT:PSS by doping it with xylitol first and then post treating it with methanesulfonic acid to improve its optical, electrical, and morphological properties.[160] When the modified PEDOT:PSS served as flexible and transparent bottom electrodes, the corresponding device based on PM6:Y6 demonstrated a high PCE of 10.5% with an AVT of 21% and remarkable mechanical stability. Interestingly, the flexible ST-OSCs were applied as a part in a simulated greenhouse and had no adverse effect on the growth of plants. Li *et al.* proposed a "welding" strategy and added Al-doped ZnO (AZO) into an AgNW network *via* a capillary force effect, to obtain a flexible and transparent electrode.[161] However, the substrate was also modified by embedding it with AgNW (Em-Ag) to enhance the adhesion of the electrode. As a result, the flexible OSCs achieved an outstanding PCE of 15.2% (Table 4).

4. Conclusions and outlooks

In the last two years, the development of electron-deficient-core-based NFAs (Y6 and its derivatives) have made a breakthrough in the field of OSCs. Due to effective exciton dissociation, negligible geminate recombination, suppressive charge recombination and excellent charge extraction of the OSCs containing PM6 and Y6, outstanding PCEs of over 17% have been attained. In order to further optimize the performance of PM6:Y6-based devices, several aspects can be considered. (1) From the aspect of matching donor materials, terpolymerization *via* accurate control of the content of the third monomer with certain functional groups is an effective and simple method. This strategy could help to properly adjust the energy levels and aggregation of donors, contributing to well-matched donor–acceptor pairs to construct high-performance devices. (2) Proper crystallinity and miscibility of the third components in constructed ternary OSCs are two other important factors in addition to complementary absorption and matching of energy levels. As reported, good miscibility between the guest donor (or acceptor) and host donor (or acceptor) is beneficial for optimizing the morphology of the active layer. Otherwise, third components with poor miscibility can also modify the morphology when the addition amount is small. (3) Reasonable processing to control the kinetics and thermodynamics during the evolution of the active layer film formation is desirable to forming a favorable morphology with nanoscale phase separation. (4) Developing the interface layer and electrode materials, which on the one hand improves the charge extraction efficiency and reduces charge recombination, and on the other hand is conducive to the development of OSCs with flexible, semi-transparent, and large-area characteristics. (5) High efficiency OSCs should also show appropriate stability under various environmental conditions. However, as various photovoltaic materials have been developed and more stable performance achieved, the required testing period has become longer, which hinders the progress of research. Investigating the mechanism of device attenuation and developing prediction methods are

urgently required. For example, Ade *et al.* established the relationships between chemical structure, intermolecular interactions and diffusion, and revealed that high activation energy and low diffusion coefficient of hypo-miscible systems are beneficial for the long-term stability of OSCs.[162] (6) A large number of photovoltaic materials have been developed, making it complex to select matching donor–acceptor pairs *via* a trial-and-error method. Driven by data science, machine learning provides a powerful and cost-effective way of learning from past data, building up structure–property relationships and then helping to fast screen materials.[163,164] In spite of the low efficiency of machine learning due to the complex nature of OSCs, it is still essential to speed up the development of OSCs.

Based on the large number of novel donor and acceptor materials, these optimization strategies could be applied to different high-efficiency and well-matched donor–acceptor pairs to further improve the photovoltaic performance of OSCs. It is expected that by integrating these optimization strategies, higher-performance and commercially viable OSCs will soon be accessible.

Conflicts of interest

There are no conflicts to declare.

Acknowledgements

The authors thank the support from the Key Research Program of Frontier Sciences, Chinese Academy of Sciences (Grant No. QYZDB-SSW-SLH033), the Outstanding Talent Research Fund of Zhengzhou University (32340035, 32340097, 32340100), and the National Natural Science Foundation of China (NSFC, No. 21875052, 52073067, 51873044, 51973146), Collaborative Innovation Center of Suzhou Nano Science & Technology, the Priority Academic Program Development of Jiangsu Higher Education Institutions.

References

1 J. Hou, O. Inganas, R. H. Friend and F. Gao, Organic solar cells based on non-fullerene acceptors, *Nat. Mater.*, 2018, **17**, 119–128.
2 D. Di Carlo Rasi and R. A. J. Janssen, Advances in solution-processed multijunction organic solar cells, *Adv. Mater.*, 2019, **31**, 1806499.
3 O. Ostroverkhova, Organic optoelectronic materials: Mechanisms and applications, *Chem. Rev.*, 2016, **116**, 13279–13412.
4 P. Cheng, G. Li, X. Zhan and Y. Yang, Next-generation organic photovoltaics based on non-fullerene acceptors, *Nat. Photonics*, 2018, **12**, 131–142.
5 S. Dai and X. Zhan, Nonfullerene acceptors for semitransparent organic solar cells, *Adv. Energy Mater.*, 2018, **8**, 1800002.
6 G. Yu, J. Gao, J. C. Hummelen, F. Wudl and A. J. Heeger, Polymer photovoltaic cells: enhanced efficiencies *via* a network of internal donor–acceptor heterojunctions, *Science*, 1995, **270**, 1789–1791.
7 J. Roncali, Molecular bulk heterojunctions: an emerging approach to organic solar cells, *Acc. Chem. Res.*, 2009, **42**, 1719–1730.
8 J. Chen and Y. Cao, Development of novel conjugated donor heterojunction photovoltaic devices, *Acc. Chem. Res.*, 2009, **42**, 1709–1718.
9 A. Karki, J. Vollbrecht, A. J. Gillett, S. S. Xiao, Y. Yang, Z. Peng, N. Schopp, A. L. Dixon, S. Yoon, M. Schrock, H. Ade, G. N. M. Reddy, R. H. Friend and T.-Q. Nguyen, The role of bulk and interfacial morphology in charge generation, recombination, and extraction in non-fullerene acceptor organic solar cells, *Energy Environ. Sci.*, 2020, **13**, 3679–3692.
10 K. Jiang, Q. Y. Wei, J. Y. L. Lai, Z. X. Peng, H. Kim, J. Yuan, L. Ye, H. Ade, Y. P. Zou and H. Yan, Alkyl chain tuning of small molecule acceptors for efficient organic solar cells, *Joule*, 2019, **3**, 3020–3033.
11 Z. H. Luo, R. J. Ma, T. Liu, J. W. Yu, Y. Q. Xiao, R. Sun, G. S. Xie, J. Yuan, Y. Z. Chen, K. Chen, G. D. Chai, H. L. Sun, J. Min, J. Zhang, Y. P. Zou, C. L. Yang, X. H. Lu, F. Gao and H. Yan, Fine-tuning energy levels *via* asymmetric end groups enables polymer solar cells with efficiencies over 17%, *Joule*, 2020, **4**, 1236–1247.
12 R. Sun, Q. Wu, J. Guo, T. Wang, Y. Wu, B. Qiu, Z. Luo, W. Yang, Z. Hu, J. Guo, M. Shi, C. Yang, F. Huang, Y. Li and J. Min, A layer-by-layer architecture for printable organic solar cells overcoming the scaling lag of module efficiency, *Joule*, 2020, **4**, 407–419.
13 Y. Cui, H. Yao, J. Zhang, T. Zhang, Y. Wang, L. Hong, K. Xian, B. Xu, S. Zhang, J. Peng, Z. Wei, F. Gao and J. Hou, Over 16% efficiency organic photovoltaic cells enabled by a chlorinated acceptor with increased open-circuit voltages, *Nat. Commun.*, 2019, **10**, 2515.
14 Q. Liu, Y. Jiang, K. Jin, J. Qin, J. Xu, W. Li, J. Xiong, J. Liu, Z. Xiao, K. Sun, S. Yang, X. Zhang and L. Ding, 18% efficiency organic solar cells, *Sci. Bull.*, 2020, **65**, 272–275.
15 J. Xiong, K. Jin, Y. F. Jiang, J. Q. Qin, T. Wang, J. F. Liu, Q. S. Liu, H. L. Peng, X. F. Li, A. X. Sun, X. Y. Meng, L. X. Zhang, L. Liu, W. T. Li, Z. M. Fang, X. Jia, Z. Xiao, Y. Q. Feng, X. T. Zhang, K. Sun, S. F. Yang, S. W. Shi and L. M. Ding, Thiolactone copolymer donor gifts organic solar cells a 16.72% efficiency, *Sci. Bull.*, 2019, **64**, 1573–1576.
16 H. Fu, W. Gao, Y. Li, F. Lin, X. Wu, J. H. Son, J. Luo, H. Y. Woo, Z. Zhu and A. K. Y. Jen, A generally applicable approach using sequential deposition to enable highly efficient organic solar cells, *Small Methods*, 2020, **4**, 2000687.
17 Y. Cui, H. Yao, J. Zhang, K. Xian, T. Zhang, L. Hong, Y. Wang, Y. Xu, K. Ma, C. An, C. He, Z. Wei, F. Gao and J. Hou, Single-junction organic photovoltaic cells with approaching 18% efficiency, *Adv. Mater.*, 2020, **32**, 1908205.

18 Y. Li, Fullerene-bisadduct acceptors for polymer solar cells, *Chem. – Asian J.*, 2013, **8**, 2316–2328.
19 X. Guo, C. Cui, M. Zhang, L. Huo, Y. Huang, J. Hou and Y. Li, High efficiency polymer solar cells based on poly (3-hexylthiophene)/indene-C70 bisadduct with solvent additive, *Energy Environ. Sci.*, 2012, **5**, 7943–7949.
20 H.-W. Luo and Z.-T. Liu, Recent developments of di-amide/imide-containing small molecular non-fullerene acceptors for organic solar cells, *Chin. Chem. Lett.*, 2016, **27**, 1283–1292.
21 J. Liu, S. Chen, D. Qian, B. Gautam, G. Yang, J. Zhao, J. Bergqvist, F. Zhang, W. Ma, H. Ade, O. Inganäs, K. Gundogdu, F. Gao and H. Yan, Fast charge separation in a non-fullerene organic solar cell with a small driving force, *Nat. Energy*, 2016, **1**, 16089.
22 C. Yan, S. Barlow, Z. Wang, H. Yan, A. K. Y. Jen, S. R. Marder and X. Zhan, Non-fullerene acceptors for organic solar cells, *Nat. Rev. Mater.*, 2018, **3**, 18003.
23 Y. Q. Pan and G. Y. Sun, Star-shaped non-fullerene small acceptors for organic solar cells, *ChemSusChem*, 2019, **12**, 4570–4600.
24 Y. Ji, L. Xu, X. Hao and K. Gao, Energy loss in organic solar cells: Mechanisms, strategies, and prospects, *Sol. RRL*, 2020, **4**, 2000130.
25 R. Zhao, J. Liu and L. Wang, Polymer acceptors containing B ← N units for organic photovoltaics, *Acc. Chem. Res.*, 2020, **53**, 1557–1567.
26 Y. W. Ji, L. X. Xu, X. T. Hao and K. Gao, Energy loss in organic solar cells: Mechanisms, strategies, and prospects, *Sol. RRL*, 2020, **4**, 2000130.
27 Y. Xie and H. Wu, Balancing charge generation and voltage loss toward efficient nonfullerene organic solar cells, *Mater. Today Adv.*, 2020, **5**, 100048.
28 W. Gao, M. Zhang, T. Liu, R. Ming, Q. An, K. Wu, D. Xie, Z. Luo, C. Zhong, F. Liu, F. Zhang, H. Yan and C. Yang, Asymmetrical ladder-type donor-induced polar small molecule acceptor to promote fill factors approaching 77% for high-performance nonfullerene polymer solar cells, *Adv. Mater.*, 2018, **30**, 1800052.
29 J. Wang, W. Wang, X. Wang, Y. Wu, Q. Zhang, C. Yan, W. Ma, W. You and X. Zhan, Enhancing performance of nonfullerene acceptors *via* side-chain conjugation strategy, *Adv. Mater.*, 2017, **29**, 1702125.
30 B. Kan, H. Feng, X. Wan, F. Liu, X. Ke, Y. Wang, Y. Wang, H. Zhang, C. Li, J. Hou and Y. Chen, Small-molecule acceptor based on the heptacyclic benzodi(cyclopentadithiophene) unit for highly efficient nonfullerene organic solar cells, *J. Am. Chem. Soc.*, 2017, **139**, 4929–4934.
31 W. Zhao, D. Qian, S. Zhang, S. Li, O. Inganäs, F. Gao and J. Hou, Fullerene-free polymer solar cells with over 11% efficiency and excellent thermal stability, *Adv. Mater.*, 2016, **28**, 4734–4739.
32 A. Wadsworth, M. Moser, A. Marks, M. S. Little, N. Gasparini, C. J. Brabec, D. Baran and I. McCulloch, Critical review of the molecular design progress in non-fullerene electron acceptors towards commercially viable organic solar cells, *Chem. Soc. Rev.*, 2019, **48**, 1596–1625.
33 Q. Guo, R. Ma, J. Hu, Z. Wang, H. Sun, X. Dong, Z. Luo, T. Liu, X. Guo, X. Guo, H. Yan, F. Liu and M. Zhang, Over 15% efficiency polymer solar cells enabled by conformation tuning of newly designed asymmetric small-molecule acceptors, *Adv. Funct. Mater.*, 2020, **30**, 2000383.
34 J. Yuan, Y. Zhang, L. Zhou, G. Zhang, H.-L. Yip, T.-K. Lau, X. Lu, C. Zhu, H. Peng, P. A. Johnson, M. Leclerc, Y. Cao, J. Ulanski, Y. Li and Y. Zou, Single-junction organic solar cell with over 15% efficiency using fused-ring acceptor with electron-deficient core, *Joule*, 2019, **3**, 1140–1151.
35 Z. Zhou, W. Liu, G. Zhou, M. Zhang, D. Qian, J. Zhang, S. Chen, S. Xu, C. Yang, F. Gao, H. Zhu, F. Liu and X. Zhu, Subtle molecular tailoring induces significant morphology optimization enabling over 16% efficiency organic solar cells with efficient charge generation, *Adv. Mater.*, 2020, **32**, 1906324.
36 S. Liu, J. Yuan, W. Deng, M. Luo, Y. Xie, Q. Liang, Y. Zou, Z. He, H. Wu and Y. Cao, High-efficiency organic solar cells with low non-radiative recombination loss and low energetic disorder, *Nat. Photonics*, 2020, **14**, 300–305.
37 J. Yuan, C. Zhang, H. Chen, C. Zhu, S. H. Cheung, B. Qiu, F. Cai, Q. Wei, W. Liu, H. Yin, R. Zhang, J. Zhang, Y. Liu, H. Zhang, W. Liu, H. Peng, J. Yang, L. Meng, F. Gao, S. So, Y. Li and Y. Zou, Understanding energetic disorder in electron-deficient-core-based non-fullerene solar cells, *Sci. China: Chem.*, 2020, **63**, 1159–1168.
38 R. Ma, T. Liu, Z. Luo, Q. Guo, Y. Xiao, Y. Chen, X. Li, S. Luo, X. Lu, M. Zhang, Y. Li and H. Yan, Improving open-circuit voltage by a chlorinated polymer donor endows binary organic solar cells efficiencies over 17%, *Sci. China: Chem.*, 2020, **63**, 325–330.
39 Z. Wang, Z. Peng, Z. Xiao, D. Seyitliyev, K. Gundogdu, L. Ding and H. Ade, Thermodynamic properties and molecular packing explain performance and processing procedures of three D18:NFA organic solar cells, *Adv. Mater.*, 2020, **32**, 2005386.
40 J. Yang, P. Cong, L. Chen, X. Wang, J. Li, A. Tang, B. Zhang, Y. Geng and E. Zhou, Introducing fluorine and sulfur atoms into quinoxaline-based p-type polymers to gradually improve the performance of fullerene-free organic solar cells, *ACS Macro Lett.*, 2019, **8**, 743–748.
41 A. Tang, Q. Zhang, M. Du, G. Li, Y. Geng, J. Zhang, Z. Wei, X. Sun and E. Zhou, Molecular engineering of D−π–A copolymers based on 4,8-bis(4-chlorothiophen-2-yl)benzo[1,2-*b*:4,5-*b*′]dithiophene (BDT-T-Cl) for high-performance fullerene-free organic solar cells, *Macromolecules*, 2019, **52**, 6227–6233.
42 F. Li, A. Tang, B. Zhang and E. Zhou, Indacenodithieno[3,2-*b*]thiophene-based wide bandgap D–π–A copolymer for nonfullerene organic solar cells, *ACS Macro Lett.*, 2019, **8**, 1599–1604.
43 Y. Chen, Y. Geng, A. Tang, X. Wang, Y. Sun and E. Zhou, Changing the π-bridge from thiophene to thieno[3,2-*b*]thiophene for the D–π–A type polymer enables high performance fullerene-free organic solar cells, *Chem. Commun.*, 2019, **55**, 6708–6710.

44 S. X. Li, C. Z. Li, M. M. Shi and H. Z. Chen, New phase for organic solar cell research: Emergence of y-series electron acceptors and their perspectives, *ACS Energy Lett.*, 2020, **5**, 1554–1567.

45 P. Cheng, J. Y. Wang, X. W. Zhan and Y. Yang, Constructing high-performance organic photovoltaics *via* emerging non-fullerene acceptors and tandem-junction structure, *Adv. Energy Mater.*, 2020, **10**, 2000746.

46 A. Karki, A. J. Gillett, R. H. Friend and T. Q. Nguyen, The path to 20% power conversion efficiencies in nonfullerene acceptor organic solar cells, *Adv. Energy Mater.*, 2020, **10**, 2003441.

47 L. Ma, S. Zhang, J. Wang, Y. Xu and J. Hou, Recent advances in non-fullerene organic solar cells: From lab to fab, *Chem. Commun.*, 2020, **56**, 14337–14352.

48 X. Y. Gao, Y. J. Wu, Y. T. Tao and W. Huang, Conjugated random terpolymer donors towards high-efficiency polymer solar cells, *Chin. J. Chem.*, 2020, **38**, 601–624.

49 J. J. Zhao, C. Yao, M. U. Ali, J. S. Miao and H. Meng, Recent advances in high-performance organic solar cells enabled by acceptor–donor–acceptor–donor–acceptor (A–DA′D–A) type acceptors, *Mater. Chem. Front.*, 2020, **4**, 3487–3504.

50 B. Zheng, L. J. Huo and Y. F. Li, Benzodithiophenedione-based polymers: Recent advances in organic photovoltaics, *NPG Asia Mater.*, 2020, **12**, 3.

51 W. A. Adeosun, D. F. Katowah, A. M. Asiri and M. A. Hussein, Conducting terpolymers and its hybrid nanocomposites variable trends. From synthesis to applications. a review, *Polym.-Plast. Technol. Mater.*, 2021, **60**, 271–285.

52 Q. Y. Wei, W. Liu, M. Leclerc, J. Yuan, H. G. Chen and Y. P. Zou, A–DA′D–A non-fullerene acceptors for high-performance organic solar cells, *Sci. China: Chem.*, 2020, **63**, 1352–1366.

53 M. Zhang, X. Guo, W. Ma, H. Ade and J. Hou, A large-bandgap conjugated polymer for versatile photovoltaic applications with high performance, *Adv. Mater.*, 2015, **27**, 4655–4660.

54 H. Zhang, H. Yao, J. Hou, J. Zhu, J. Zhang, W. Li, R. Yu, B. Gao, S. Zhang and J. Hou, Over 14% efficiency in organic solar cells enabled by chlorinated nonfullerene small-molecule acceptors, *Adv. Mater.*, 2018, **30**, 1800613.

55 T. Liu, Z. H. Luo, Q. P. Fan, G. Y. Zhang, L. Zhang, W. Gao, X. Guo, W. Ma, M. J. Zhang, C. L. Yang, Y. F. Li and H. Yan, Use of two structurally similar small molecular acceptors enabling ternary organic solar cells with high efficiencies and fill factors, *Energy Environ. Sci.*, 2018, **11**, 3275–3282.

56 Q. Guo, J. Lin, H. Q. Liu, X. L. Dong, X. Guo, L. Ye, Z. F. Ma, Z. Tang, H. Ade, M. J. Zhang and Y. F. Li, Asymmetrically noncovalently fused-ring acceptor for high-efficiency organic solar cells with reduced voltage loss and excellent thermal stability, *Nano Energy*, 2020, **74**, 104861.

57 Q. P. Fan, W. Y. Su, Y. Wang, B. Guo, Y. F. Jiang, X. Guo, F. Liu, T. P. Russell, M. J. Zhang and Y. F. Li, Synergistic effect of fluorination on both donor and acceptor materials for high performance non-fullerene polymer solar cells with 13.5% efficiency, *Sci. China: Chem.*, 2018, **61**, 531–537.

58 H. Sun, H. Yu, Y. Shi, J. Yu, Z. Peng, X. Zhang, B. Liu, J. Wang, R. Singh, J. Lee, Y. Li, Z. Wei, Q. Liao, Z. Kan, L. Ye, H. Yan, F. Gao and X. Guo, A narrow-bandgap n-type polymer with an acceptor-acceptor backbone enabling efficient all-polymer solar cells, *Adv. Mater.*, 2020, **32**, 2004183.

59 H. T. Yao, L. K. Ma, H. Yu, J. W. Yu, P. C. Y. Chow, W. Y. Xue, X. H. Zou, Y. Z. Chen, J. E. Liang, L. Arunagiri, F. Gao, H. L. Sun, G. Y. Zhang, W. Ma and H. Yan, All-polymer solar cells with over 12% efficiency and a small voltage loss enabled by a polymer acceptor based on an extended fused ring core, *Adv. Energy Mater.*, 2020, **10**, 2001408.

60 J. N. Wu, Y. Meng, X. Guo, L. Zhu, F. Liu and M. J. Zhang, All-polymer solar cells based on a novel narrow-bandgap polymer acceptor with power conversion efficiency over 10%, *J. Mater. Chem. A*, 2019, **7**, 16190–16196.

61 H. J. Snaith, How should you measure your excitonic solar cells?, *Energy Environ. Sci.*, 2012, **5**, 6513.

62 M. Green, E. Dunlop, J. Hohl-Ebinger, M. Yoshita, N. Kopidakis and X. Hao, Solar cell efficiency tables (version 57), *Prog. Photovoltaics Res. Appl.*, 2020, **29**, 3–15.

63 E. Zimmermann, P. Ehrenreich, T. Pfadler, J. A. Dorman, J. Weickert and L. Schmidt-Mende, Erroneous efficiency reports harm organic solar cell research, *Nat. Photonics*, 2014, **8**, 669–672.

64 A. Gavrik, A. L. Mannanov, S. Tsarev, V. V. Bruevich, V. A. Trukhanov, Y. A. Chernikov, P. S. Savchenko, J. D. Gvozdkova, A. N. Solodukhin, P. A. Troshin, S. A. Ponomarenko and D. Y. Paraschuk, Spectral technique for accurate efficiency measurements of emerging solar cells, *Sol. Energy*, 2020, **206**, 770–777.

65 A. Karki, J. Vollbrecht, A. L. Dixon, N. Schopp, M. Schrock, G. N. M. Reddy and T. Q. Nguyen, Understanding the high performance of over 15% efficiency in single-junction bulk heterojunction organic solar cells, *Adv. Mater.*, 2019, **31**, 1903868.

66 A. Tang, W. Song, B. Xiao, J. Guo, J. Min, Z. Ge, J. Zhang, Z. Wei and E. Zhou, Benzotriazole-based acceptor and donors, coupled with chlorination, achieve a high V_{oc} of 1.24 V and an efficiency of 10.5% in fullerene-free organic solar cells, *Chem. Mater.*, 2019, **31**, 3941–3947.

67 N. An, Y. Cai, H. Wu, A. Tang, K. Zhang, X. Hao, Z. Ma, Q. Guo, H. S. Ryu, H. Y. Woo, Y. Sun and E. Zhou, Solution-processed organic solar cells with high open-circuit voltage of 1.3 v and low non-radiative voltage loss of 0.16 V, *Adv. Mater.*, 2020, **32**, 2002122.

68 J. Wu, J. Lee, Y.-C. Chin, H. Yao, H. Cha, J. Luke, J. Hou, J.-S. Kim and J. R. Durrant, Exceptionally low charge trapping enables highly efficient organic bulk heterojunction solar cells, *Energy Environ. Sci.*, 2020, **13**, 2422–2430.

69 S. Chen, Y. Wang, L. Zhang, J. Zhao, Y. Chen, D. Zhu, H. Yao, G. Zhang, W. Ma, R. H. Friend, P. C. Y. Chow, F. Gao and H. Yan, Efficient nonfullerene organic solar cells with small driving forces for both hole and electron transfer, *Adv. Mater.*, 2018, **30**, 1804215.

70 A. Y. Sosorev, D. Y. Godovsky and D. Y. Paraschuk, Hot kinetic model as a guide to improve organic photovoltaic materials, *Phys. Chem. Chem. Phys.*, 2018, **20**, 3658–3671.
71 H. Tamura and I. Burghardt, Ultrafast charge separation in organic photovoltaics enhanced by charge delocalization and vibronically hot exciton dissociation, *J. Am. Chem. Soc.*, 2013, **135**, 16364–16367.
72 L. Perdigon-Toro, H. Zhang, A. Markina, J. Yuan, S. M. Hosseini, C. M. Wolff, G. Zuo, M. Stolterfoht, Y. Zou, F. Gao, D. Andrienko, S. Shoaee and D. Neher, Barrierless free charge generation in the high-performance PM6:Y6 bulk heterojunction non-fullerene solar cell, *Adv. Mater.*, 2020, **32**, 1906763.
73 Z. Tu, G. Han and Y. Yi, Barrier-free charge separation enabled by electronic polarization in high-efficiency non-fullerene organic solar cells, *J. Phys. Chem. Lett.*, 2020, **11**, 2585–2591.
74 S. Karuthedath, J. Gorenflot, Y. Firdaus, N. Chaturvedi, C. S. P. De Castro, G. T. Harrison, J. I. Khan, A. Markina, A. H. Balawi, T. A. D. Pena, W. Liu, R. Z. Liang, A. Sharma, S. H. K. Paleti, W. Zhang, Y. Lin, E. Alarousu, D. H. Anjum, P. M. Beaujuge, S. De Wolf, I. McCulloch, T. D. Anthopoulos, D. Baran, D. Andrienko and F. Laquai, Intrinsic efficiency limits in low-bandgap non-fullerene acceptor organic solar cells, *Nat. Mater.*, 2021, **20**, 378–384.
75 R. Wang, C. Zhang, Q. Li, Z. Zhang, X. Wang and M. Xiao, Charge separation from an intra-moiety intermediate state in the high-performance PM6:Y6 organic photovoltaic blend, *J. Am. Chem. Soc.*, 2020, **142**, 12751–12759.
76 M. T. Seifrid, G. N. M. Reddy, C. Zhou, B. F. Chmelka and G. C. Bazan, Direct observation of the relationship between molecular topology and bulk morphology for a pi-conjugated material, *J. Am. Chem. Soc.*, 2019, **141**, 5078–5082.
77 M. Seifrid, G. N. M. Reddy, B. F. Chmelka and G. C. Bazan, Insight into the structures and dynamics of organic semiconductors through solid-state NMR spectroscopy, *Nat. Rev. Mater.*, 2020, **5**, 910–930.
78 W. Zhu, A. P. Spencer, S. Mukherjee, J. M. Alzola, V. K. Sangwan, S. H. Amsterdam, S. M. Swick, L. O. Jones, M. C. Heiber, A. A. Herzing, G. Li, C. L. Stern, D. M. DeLongchamp, K. L. Kohlstedt, M. C. Hersam, G. C. Schatz, M. R. Wasielewski, L. X. Chen, A. Facchetti and T. J. Marks, Crystallography, morphology, electronic structure, and transport in non-fullerene/non-indacenodithienothiophene polymer:Y6 solar cells, *J. Am. Chem. Soc.*, 2020, **142**, 14532–14547.
79 L. Zhu, M. Zhang, G. Zhou, T. Hao, J. Xu, J. Wang, C. Qiu, N. Prine, J. Ali, W. Feng, X. Gu, Z. Ma, Z. Tang, H. Zhu, L. Ying, Y. Zhang and F. Liu, Efficient organic solar cell with 16.88% efficiency enabled by refined acceptor crystallization and morphology with improved charge transfer and transport properties, *Adv. Energy Mater.*, 2020, **10**, 1904234.
80 G. Zhang, X. K. Chen, J. Xiao, P. C. Y. Chow, M. Ren, G. Kupgan, X. Jiao, C. C. S. Chan, X. Du, R. Xia, Z. Chen, J. Yuan, Y. Zhang, S. Zhang, Y. Liu, Y. Zou, H. Yan, K. S. Wong, V. Coropceanu, N. Li, C. J. Brabec, J. L. Bredas, H. L. Yip and Y. Cao, Delocalization of exciton and electron wavefunction in non-fullerene acceptor molecules enables efficient organic solar cells, *Nat. Commun.*, 2020, **11**, 3943.
81 V. Coropceanu, J. Cornil, Demetrio A. da Silva Filho, R. S. Yoann Olivier and J.-L. Brédas, Charge transport in organic semiconductors, *Chem. Rev.*, 2007, **107**, 926–952.
82 J. L. Bredas, J. P. Calbert, D. A. da Silva Filho and J. Cornil, Organic semiconductors: A theoretical characterization of the basic parameters governing charge transport, *Proc. Natl. Acad. Sci. U. S. A.*, 2002, **99**, 5804–5809.
83 D. Gedefaw, X. Pan and M. R. Andersson, Recent advances in the synthesis of electron donor conjugated terpolymers for solar cell applications, *Front. Mater.*, 2020, **7**, 280.
84 Q. Bian, B. A. Abdulahi, Z. Genene, E. Wang, W. Mammo and O. Inganas, Reduced nonradiative voltage loss in terpolymer solar cells, *J. Phys. Chem. Lett.*, 2020, **11**, 3796–3802.
85 Y. Cui, H. Yao, L. Hong, T. Zhang, Y. Xu, K. Xian, B. Gao, J. Qin, J. Zhang, Z. Wei and J. Hou, Achieving over 15% efficiency in organic photovoltaic cells *via* copolymer design, *Adv. Mater.*, 2019, **31**, 1808356.
86 L. Hong, H. Yao, Z. Wu, Y. Cui, T. Zhang, Y. Xu, R. Yu, Q. Liao, B. Gao, K. Xian, H. Y. Woo, Z. Ge and J. Hou, Eco-compatible solvent-processed organic photovoltaic cells with over 16% efficiency, *Adv. Mater.*, 2019, **31**, 1903441.
87 H. Sun, T. Liu, J. Yu, T.-K. Lau, G. Zhang, Y. Zhang, M. Su, Y. Tang, R. Ma, B. Liu, J. Liang, K. Feng, X. Lu, X. Guo, F. Gao and H. Yan, A monothiophene unit incorporating both fluoro and ester substitution enabling high-performance donor polymers for non-fullerene solar cells with 16.4% efficiency, *Energy Environ. Sci.*, 2019, **12**, 3328–3337.
88 J. Liang, M. Pan, G. Chai, Z. Peng, J. Zhang, S. Luo, Q. Han, Y. Chen, A. Shang, F. Bai, Y. Xu, H. Yu, J. Y. L. Lai, Q. Chen, M. Zhang, H. Ade and H. Yan, Random polymerization strategy leads to a family of donor polymers enabling well-controlled morphology and multiple cases of high-performance organic solar cells, *Adv. Mater.*, 2020, **32**, 2003500.
89 X. Guo, Q. Fan, J. Wu, G. Li, Z. Peng, W. Su, J. Lin, L. Hou, Y. Qin, H. Ade, L. Ye, M. Zhang and Y. Li, Optimized active layer morphologies *via* ternary copolymerization of polymer donors for 17.6% efficiency organic solar cells with enhanced fill factor, *Angew. Chem., Int. Ed.*, 2021, **60**, 2322–2329.
90 J. Wu, G. Li, J. Fang, X. Guo, L. Zhu, B. Guo, Y. Wang, G. Zhang, L. Arunagiri, F. Liu, H. Yan, M. Zhang and Y. Li, Random terpolymer based on thiophene–thiazolothiazole unit enabling efficient non-fullerene organic solar cells, *Nat. Commun.*, 2020, **11**, 4612.
91 W. Xu, M. Zhang, J. Xiao, M. Zeng, L. Ye, C. Weng, B. Zhao, J. Zhang and S. Tan, Improved photovoltaic properties of PM6-based terpolymer donors containing benzothiadiazole

with a siloxane-terminated side chain, *Polym. Chem.*, 2020, **11**, 6178–6186.

92 R. Sun, T. Wang, Z. Luo, Z. Hu, F. Huang, C. Yang and J. Min, Achieving eco-compatible organic solar cells with efficiency >16.5% based on an iridium complex-incorporated polymer donor, *Sol. RRL*, 2020, **4**, 2000156.

93 X. Li, R. Ma, T. Liu, Y. Xiao, G. Chai, X. Lu, H. Yan and Y. Li, Fine-tuning homo energy levels between PM6 and PBDB-T polymer donors *via* ternary copolymerization, *Sci. China: Chem.*, 2020, **63**, 1256–1261.

94 D. Li, L. Zhu, X. Liu, W. Xiao, J. Yang, R. Ma, L. Ding, F. Liu, C. Duan, M. Fahlman and Q. Bao, Enhanced and balanced charge transport boosting ternary solar cells over 17% efficiency, *Adv. Mater.*, 2020, **32**, 2002344.

95 C. Yan, H. Tang, R. Ma, M. Zhang, T. Liu, J. Lv, J. Huang, Y. Yang, T. Xu, Z. Kan, H. Yan, F. Liu, S. Lu and G. Li, Synergy of liquid-crystalline small-molecule and polymeric donors delivers uncommon morphology evolution and 16.6% efficiency organic photovoltaics, *Adv. Sci.*, 2020, **7**, 2000149.

96 X. Chen, Q. Zhang, D. Wang, X. Xu, Z. Wang, Y. Li, H. Zhu, X. Lu, W. Chen, H. Qiu and C.-Z. Li, High-efficiency ternary organic solar cells based on the synergized polymeric and small-molecule donors, *Sol. RRL*, 2020, **4**, 2000537.

97 S. Chen, T. Yan, B. Fanady, W. Song, J. Ge, Q. Wei, R. Peng, G. Chen, Y. Zou and Z. Ge, High efficiency ternary organic solar cells enabled by compatible dual-donor strategy with planar conjugated structures, *Sci. China: Chem.*, 2020, **63**, 917–923.

98 T. Yan, J. Ge, T. Lei, W. Zhang, W. Song, B. Fanady, D. Zhang, S. Chen, R. Peng and Z. Ge, 16.55% efficiency ternary organic solar cells enabled by incorporating a small molecular donor, *J. Mater. Chem. A*, 2019, **7**, 25894–25899.

99 Q. An, J. Wang, X. Ma, J. Gao, Z. Hu, B. Liu, H. Sun, X. Guo, X. Zhang and F. Zhang, Two compatible polymer donors contribute synergistically for ternary organic solar cells with 17.53% efficiency, *Energy Environ. Sci.*, 2020, **13**, 5039–5047.

100 G. Xie, Z. Zhang, Z. Su, X. Zhang and J. Zhang, 16.5% efficiency ternary organic photovoltaics with two polymer donors by optimizing molecular arrangement and phase separation, *Nano Energy*, 2020, **69**, 104447.

101 Y. Tang, J. Yu, H. Sun, Z. Wu, C. W. Koh, X. Wu, B. Liu, J. Wang, Q. Liao, Y. Li, H. Guo, H. Y. Woo, F. Gao and X. Guo, Two compatible polymer donors enabling ternary organic solar cells with a small nonradiative energy loss and broad composition tolerance, *Sol. RRL*, 2020, **4**, 2000396.

102 Y. Chang, T.-K. Lau, P. C. Y. Chow, N. Wu, D. Su, W. Zhang, H. Meng, C. Ma, T. Liu, K. Li, X. Zou, K. S. Wong, X. Lu, H. Yan and C. Zhan, A 16.4% efficiency organic photovoltaic cell enabled using two donor polymers with their side-chains oriented differently by a ternary strategy, *J. Mater. Chem. A*, 2020, **8**, 3676–3685.

103 J. Han, X. Wang, D. Huang, C. Yang, R. Yang and X. Bao, Employing asymmetrical thieno[3,4-*d*]pyridazin-1(2h)-one block enables efficient ternary polymer solar cells with improved light-harvesting and morphological properties, *Macromolecules*, 2020, **53**, 6619–6629.

104 B. H. Jiang, Y. P. Wang, C. Y. Liao, Y. M. Chang, Y. W. Su, R. J. Jeng and C. P. Chen, Improved blend film morphology and free carrier generation provide a high-performance ternary polymer solar cell, *ACS Appl. Mater. Interfaces*, 2021, **13**, 1076–1085.

105 R. Yu, H. Yao, Y. Cui, L. Hong, C. He and J. Hou, Improved charge transport and reduced nonradiative energy loss enable over 16% efficiency in ternary polymer solar cells, *Adv. Mater.*, 2019, **31**, 1902302.

106 M.-A. Pan, T.-K. Lau, Y. Tang, Y.-C. Wu, T. Liu, K. Li, M.-C. Chen, X. Lu, W. Ma and C. Zhan, 16.7%-efficiency ternary blended organic photovoltaic cells with PCBM as the acceptor additive to increase the open-circuit voltage and phase purity, *J. Mater. Chem. A*, 2019, **7**, 20713–20722.

107 T. Yan, W. Song, J. Huang, R. Peng, L. Huang and Z. Ge, 16.67% rigid and 14.06% flexible organic solar cells enabled by ternary heterojunction strategy, *Adv. Mater.*, 2019, **31**, 1902210.

108 S. He, Z. Shen, J. Yu, H. Guan, G. Lu, T. Xiao, S. Yang, Y. Zou and L. Bu, Vertical miscibility of bulk heterojunction films contributes to high photovoltaic performance, *Adv. Mater. Interfaces*, 2020, **7**, 2000577.

109 S. Li, L. Zhan, Y. Jin, G. Zhou, T. K. Lau, R. Qin, M. Shi, C. Z. Li, H. Zhu, X. Lu, F. Zhang and H. Chen, Asymmetric electron acceptors for high-efficiency and low-energy-loss organic photovoltaics, *Adv. Mater.*, 2020, **32**, 2001160.

110 T. Liu, R. Ma, Z. Luo, Y. Guo, G. Zhang, Y. Xiao, T. Yang, Y. Chen, G. Li, Y. Yi, X. Lu, H. Yan and B. Tang, Concurrent improvement in J_{sc} and V_{oc} in high-efficiency ternary organic solar cells enabled by a red-absorbing small-molecule acceptor with a high LUMO level, *Energy Environ. Sci.*, 2020, **13**, 2115–2123.

111 L. Zhan, S. Li, T.-K. Lau, Y. Cui, X. Lu, M. Shi, C.-Z. Li, H. Li, J. Hou and H. Chen, Over 17% efficiency ternary organic solar cells enabled by two non-fullerene acceptors working in an alloy-like model, *Energy Environ. Sci.*, 2020, **13**, 635–645.

112 J. Song, C. Li, L. Zhu, J. Guo, J. Xu, X. Zhang, K. Weng, K. Zhang, J. Min, X. Hao, Y. Zhang, F. Liu and Y. Sun, Ternary organic solar cells with efficiency >16.5% based on two compatible nonfullerene acceptors, *Adv. Mater.*, 2019, **31**, 1905645.

113 D. Su, M.-A. Pan, Z. Liu, T.-K. Lau, X. Li, F. Shen, S. Huo, X. Lu, A. Xu, H. Yan and C. Zhan, A trialkylsilylthienyl chain-substituted small-molecule acceptor with higher LUMO level and reduced band gap for over 16% efficiency fullerene-free ternary solar cells, *Chem. Mater.*, 2019, **31**, 8908–8917.

114 K. Li, Y. Wu, Y. Tang, M. A. Pan, W. Ma, H. Fu, C. Zhan and J. Yao, Ternary blended fullerene-level acceptor to improve film morphology, *Adv. Energy Mater.*, 2019, **9**, 1901728.

115 Q. An, J. Wang, W. Gao, X. Ma, Z. Hu, J. Gao, C. Xu, M. Hao, X. Zhang, C. Yang and F. Zhang, Alloy-like ternary polymer

solar cells with over 17.2% efficiency, *Sci. Bull.*, 2020, **65**, 538–545.

116 Q. An, X. Ma, J. Gao and F. Zhang, Solvent additive-free ternary polymer solar cells with 16.27% efficiency, *Sci. Bull.*, 2019, **64**, 504–506.

117 R. Ma, T. Liu, Z. Luo, K. Gao, K. Chen, G. Zhang, W. Gao, Y. Xiao, T.-K. Lau, Q. Fan, Y. Chen, L.-K. Ma, H. Sun, G. Cai, T. Yang, X. Lu, E. Wang, C. Yang, A. K. Y. Jen and H. Yan, Adding a third component with reduced miscibility and higher LUMO level enables efficient ternary organic solar cells, *ACS Energy Lett.*, 2020, **5**, 2711–2720.

118 N. Gasparini, S. H. K. Paleti, J. Bertrandie, G. Cai, G. Zhang, A. Wadsworth, X. Lu, H.-L. Yip, I. McCulloch and D. Baran, Exploiting ternary blends for improved photostability in high-efficiency organic solar cells, *ACS Energy Lett.*, 2020, **5**, 1371–1379.

119 G. Cai, Y. Li, J. Zhou, P. Xue, K. Liu, J. Wang, Z. Xie, G. Li, X. Zhan and X. Lu, Enhancing open-circuit voltage of high-efficiency nonfullerene ternary solar cells with a star-shaped acceptor, *ACS Appl. Mater. Interfaces*, 2020, **12**, 50660–50667.

120 S. Dong, K. Zhang, T. Jia, W. Zhong, X. Wang, F. Huang and Y. Cao, Suppressing the excessive aggregation of nonfullerene acceptor in blade-coated active layer by using n-type polymer additive to achieve large-area printed organic solar cells with efficiency over 15%, *EcoMat*, 2019, **1**, 12006.

121 Y. Ma, X. Zhou, D. Cai, Q. Tu, W. Ma and Q. Zheng, A minimal benzo[*c*][1,2,5]thiadiazole-based electron acceptor as a third component material for ternary polymer solar cells with efficiencies exceeding 16.0%, *Mater. Horiz.*, 2020, **7**, 117–124.

122 X. Liao, Q. He, G. Zhou, X. Xia, P. Zhu, Z. Xing, H. Zhu, Z. Yao, X. Lu and Y. Chen, Regulating favorable morphology evolution by a simple liquid-crystalline small molecule enables organic solar cells with over 17% efficiency and a remarkable j_{sc} of 26.56 mA cm^{-2}, *Chem. Mater.*, 2021, **33**, 430–440.

123 X. Du, J. Zhao, H. Zhang, X. Lu, L. Zhou, Z. Chen, H. Lin, C. Zheng and S. Tao, Modulating the molecular packing and distribution enables fullerene-free ternary organic solar cells with high efficiency and long shelf-life, *J. Mater. Chem. A*, 2019, **7**, 20139–20150.

124 X. Du, Y. Yuan, L. Zhou, H. Lin, C. Zheng, J. Luo, Z. Chen, S. Tao and L. S. Liao, Delayed fluorescence emitter enables near 17% efficiency ternary organic solar cells with enhanced storage stability and reduced recombination energy loss, *Adv. Funct. Mater.*, 2020, **30**, 1909837.

125 X. Ma, J. Wang, Q. An, J. Gao, Z. Hu, C. Xu, X. Zhang, Z. Liu and F. Zhang, Highly efficient quaternary organic photovoltaics by optimizing photogenerated exciton distribution and active layer morphology, *Nano Energy*, 2020, **70**, 104496.

126 K. Li, Y. Wu, X. Li, H. Fu and C. Zhan, 17.1%-efficiency organic photovoltaic cell enabled with two higher-LUMO-level acceptor guests as the quaternary strategy, *Sci. China: Chem.*, 2020, **63**, 490–496.

127 M. Zhang, L. Zhu, G. Zhou, T. Hao, C. Qiu, Z. Zhao, Q. Hu, B. W. Larson, H. Zhu, Z. Ma, Z. Tang, W. Feng, Y. Zhang, T. P. Russell and F. Liu, Single-layered organic photovoltaics with double cascading charge transport pathways: 18% efficiencies, *Nat. Commun.*, 2021, **12**, 309.

128 H. Zhao, H. B. Naveed, B. Lin, X. Zhou, J. Yuan, K. Zhou, H. Wu, R. Guo, M. A. Scheel, A. Chumakov, S. V. Roth, Z. Tang, P. Muller-Buschbaum and W. Ma, Hot hydrocarbon-solvent slot-die coating enables high-efficiency organic solar cells with temperature-dependent aggregation behavior, *Adv. Mater.*, 2020, **32**, 2002302.

129 R. Zeng, S. Du, Y. Gong, Y. Bai, S. Hu, T. Hayat, A. Alsaedi and Z. Tan, Facile method of solvent-flushing to building component distribution within photoactive layers for high-performance organic solar cells, *ACS Appl. Mater. Interfaces*, 2020, **12**, 31459–31466.

130 Y. Qin, Y. Xu, Z. Peng, J. Hou and H. Ade, Low temperature aggregation transitions in N3 and Y6 acceptors enable double-annealing method that yields hierarchical morphology and superior efficiency in nonfullerene organic solar cells, *Adv. Funct. Mater.*, 2020, **30**, 2005011.

131 D. Zhang, Q. Li, J. Zhang, J. Wang, X. Zhang, R. Wang, J. Zhou, Z. Wei, C. Zhang, H. Zhou and Y. Zhang, Control of nanomorphology in fullerene-free organic solar cells by Lewis acid doping with enhanced photovoltaic efficiency, *ACS Appl. Mater. Interfaces*, 2020, **12**, 667–677.

132 Y. Lin, Y. Firdaus, M. I. Nugraha, F. Liu, S. Karuthedath, A. H. Emwas, W. Zhang, A. Seitkhan, M. Neophytou, H. Faber, E. Yengel, I. McCulloch, L. Tsetseris, F. Laquai and T. D. Anthopoulos, 17.1% efficient single-junction organic solar cells enabled by n-type doping of the bulk-heterojunction, *Adv. Sci.*, 2020, **7**, 1903419.

133 L. Liu, Y. Kan, K. Gao, J. Wang, M. Zhao, H. Chen, C. Zhao, T. Jiu, A. K. Jen and Y. Li, Graphdiyne derivative as multifunctional solid additive in binary organic solar cells with 17.3% efficiency and high reproductivity, *Adv. Mater.*, 2020, **32**, 1907604.

134 T. Yang, R. Ma, H. Cheng, Y. Xiao, Z. Luo, Y. Chen, S. Luo, T. Liu, X. Lu and H. Yan, A compatible polymer acceptor enables efficient and stable organic solar cells as a solid additive, *J. Mater. Chem. A*, 2020, **8**, 17706–17712.

135 S. M. Hosseini, N. Tokmoldin, Y. W. Lee, Y. Zou, H. Y. Woo, D. Neher and S. Shoaee, Putting order into PM6:Y6 solar cells to reduce the Langevin recombination in 400 nm thick junction, *Sol. RRL*, 2020, **4**, 2000498.

136 Q. Yang, S. Yu, P. Fu, W. Yu, Y. Liu, X. Liu, Z. Feng, X. Guo and C. Li, Boosting performance of non-fullerene organic solar cells by 2D g-C_3N_4 doped PEDOT:PSS, *Adv. Funct. Mater.*, 2020, **30**, 1910205.

137 M. Zeng, X. Wang, R. Ma, W. Zhu, Y. Li, Z. Chen, J. Zhou, W. Li, T. Liu, Z. He, H. Yan, F. Huang and Y. Cao, Dopamine semiquinone radical doped PEDOT:PSS: Enhanced conductivity, work function and performance in organic solar cells, *Adv. Energy Mater.*, 2020, **10**, 2000743.

138 H. Tang, Z. Liu, Z. Hu, Y. Liang, F. Huang and Y. Cao, Oxoammonium enabled secondary doping of hole

transporting material PEDOT:PSS for high-performance organic solar cells, *Sci. China: Chem.*, 2020, **63**, 802–809.

139 N. S. Alharbi, C. Wang, F. E. Alsaadi, S. O. Rabah and Z. A. Tan, A general approach of adjusting the surface-free energy of the interfacial layer for high-performance organic solar cells, *Adv. Sustainable Syst.*, 2020, **4**, 2000054.

140 K. Yang, S. Chen, J. Fu, S. Jung, J. Ye, Z. Kan, C. Hu, C. Yang, Z. Xiao, S. Lu and K. Sun, Molecular lock induced by chloroplatinic acid doping of PEDOT:PSS for high-performance organic photovoltaics, *ACS Appl. Mater. Interfaces*, 2020, **12**, 30954–30961.

141 J. Dong, J. Guo, X. Wang, P. Dong, Z. Wang, Y. Zhou, Y. Miao, B. Zhao, Y. Hao, H. Wang, B. Xu and S. Yin, A low-temperature solution-processed CuSCN/polymer hole transporting layer enables high efficiency for organic solar cells, *ACS Appl. Mater. Interfaces*, 2020, **12**, 46373–46380.

142 Y. Lin, B. Adilbekova, Y. Firdaus, E. Yengel, H. Faber, M. Sajjad, X. Zheng, E. Yarali, A. Seitkhan, O. M. Bakr, A. El-Labban, U. Schwingenschlogl, V. Tung, I. McCulloch, F. Laquai and T. D. Anthopoulos, 17% efficient organic solar cells based on liquid exfoliated WS_2 as a replacement for PEDOT:PSS, *Adv. Mater.*, 2019, **31**, 1902965.

143 H. N. Tran, S. Park, F. T. A. Wibowo, N. V. Krishna, J. H. Kang, J. H. Seo, H. Nguyen-Phu, S. Y. Jang and S. Cho, 17% non-fullerene organic solar cells with annealing-free aqueous MoO_x, *Adv. Sci.*, 2020, **7**, 2002395.

144 B. Liu, Y. Wang, P. Chen, X. Zhang, H. Sun, Y. Tang, Q. Liao, J. Huang, H. Wang, H. Meng and X. Guo, Boosting efficiency and stability of organic solar cells using ultralow-cost BiOCl nanoplates as hole transporting layers, *ACS Appl. Mater. Interfaces*, 2019, **11**, 33505–33514.

145 J. J. Park, Y. J. Heo, J. M. Yun, Y. Kim, S. C. Yoon, S. H. Lee and D. Y. Kim, Orthogonal printable reduced graphene oxide 2D materials as hole transport layers for high-performance inverted polymer solar cells: Sheet size effect on photovoltaic properties, *ACS Appl. Mater. Interfaces*, 2020, **12**, 42811–42820.

146 H. Xu, H. Zou, D. Zhou, G. Zeng, L. Chen, X. Liao and Y. Chen, Printable hole transport layer for 1.0 cm^2 organic solar cells, *ACS Appl. Mater. Interfaces*, 2020, **12**, 52028–52037.

147 H. Jiang, T. Li, X. Han, X. Guo, B. Jia, K. Liu, H. Cao, Y. Lin, M. Zhang, Y. Li and X. Zhan, Passivated metal oxide n-type contacts for efficient and stable organic solar cells, *ACS Appl. Energy Mater.*, 2019, **3**, 1111–1118.

148 Y. Luo, S. Fang, N. Zheng, L. Liu, F. Würthner and Z. Xie, Increased electron transport and hole blocking in an aqueous solution processed dye-doped ZnO cathode interlayer for high performance organic solar cells, *ACS Appl. Energy Mater.*, 2020, **3**, 1694–1701.

149 H. W. Cheng, P. Raghunath, K. L. Wang, P. Cheng, T. Haung, Q. Wu, J. Yuan, Y. C. Lin, H. C. Wang, Y. Zou, Z. K. Wang, M. C. Lin, K. H. Wei and Y. Yang, Potassium-presenting zinc oxide surfaces induce vertical phase separation in fullerene-free organic photovoltaics, *Nano Lett.*, 2020, **20**, 715–721.

150 F. Pan, C. Sun, Y. Li, D. Tang, Y. Zou, X. Li, S. Bai, X. Wei, M. Lv, X. Chen and Y. Li, Solution-processable n-doped graphene-containing cathode interfacial materials for high-performance organic solar cells, *Energy Environ. Sci.*, 2019, **12**, 3400–3411.

151 F. Pan, S. Bai, X. Wei, Y. Li, D. Tang, X. Chen, M. Lv and Y. Li, 3D surfactant-dispersed graphenes as cathode interfacial materials for organic solar cells, *Sci. China Mater.*, 2021, **64**, 277–287.

152 L. Tian, J. Jing, H. Tang, Y. Liang, Z. Hu, M. Rafiq, F. Huang and Y. Cao, Aldol condensation-polymerized n-doped conjugated polyelectrolytes for high-performance nonfullerene polymer solar cells, *Sol. RRL*, 2020, 2000523, DOI: 10.1002/solr.202000523.

153 Y. Bai, C. Zhao, S. Zhang, S. Zhang, R. Yu, J. Hou, Z. A. Tan and Y. Li, Printable SnO2 cathode interlayer with up to 500 nm thickness-tolerance for high-performance and large-area organic solar cells, *Sci. China: Chem.*, 2020, **63**, 957–965.

154 Y. Bai, C. Zhao, R. Shi, J. Wang, F. Wang, T. Hayat, A. Alsaedi and Z. A. Tan, Novel cathode buffer layer of $Al(acac)_3$ enables efficient, large area and stable semi-transparent organic solar cells, *Mater. Chem. Front.*, 2020, **4**, 2072–2080.

155 Y. Li, W. Song, T. Yan, J. Xiao, Y. Han, S. Chen, R. Peng, J. Zhang and Z. Ge, Enhanced efficiency of organic solar cells *via* Si-based non-conjugated small-molecule electrolyte as cathode interlayer, *Org. Electron.*, 2020, **85**, 105863.

156 S. Chen, L. Liu, X. Gao, Y. Hua, L. Peng, Y. Zhang, L. Yang, Y. Tan, F. He and H. Xia, Addition of alkynes and osmium carbynes towards functionalized DPI-PPI conjugated systems, *Nat. Commun.*, 2020, **11**, 4651.

157 Y. Xiong, R. E. Booth, T. Kim, L. Ye, Y. Liu, Q. Dong, M. Zhang, F. So, Y. Zhu, A. Amassian, B. T. O'Connor and H. Ade, Novel bimodal silver nanowire network as top electrodes for reproducible and high-efficiency semitransparent organic photovoltaics, *Sol. RRL*, 2020, **4**, 2000328.

158 B. H. Jiang, H. E. Lee, J. H. Lu, T. H. Tsai, T. S. Shieh, R. J. Jeng and C. P. Chen, High-performance semitransparent organic photovoltaics featuring a surface phase-matched transmission-enhancing Ag/ITO electrode, *ACS Appl. Mater. Interfaces*, 2020, **12**, 39496–39504.

159 Z. Hu, Z. Wang, Q. An and F. Zhang, Semitransparent polymer solar cells with 12.37% efficiency and 18.6% average visible transmittance, *Sci. Bull.*, 2020, **65**, 131–137.

160 W. Song, B. Fanady, R. Peng, L. Hong, L. Wu, W. Zhang, T. Yan, T. Wu, S. Chen and Z. Ge, Foldable semitransparent organic solar cells for photovoltaic and photosynthesis, *Adv. Energy Mater.*, 2020, **10**, 2000136.

161 X. Chen, G. Xu, G. Zeng, H. Gu, H. Chen, H. Xu, H. Yao, Y. Li, J. Hou and Y. Li, Realizing ultrahigh mechanical flexibility and >15% efficiency of flexible organic solar cells *via* a "welding" flexible transparent electrode, *Adv. Mater.*, 2020, **32**, 1908478.

162 M. Ghasemi, N. Balar, Z. Peng, H. Hu, Y. Qin, T. Kim, J. J. Rech, M. Bidwell, W. Mask, I. McCulloch, W. You, A. Amassian, C. Risko, B. T. O'Connor and H. Ade, A molecular interaction-diffusion framework for predicting

organic solar cell stability, *Nat. Mater.*, 2021, DOI: 10.1038/s41563-020-00872-6.

163 A. Mahmood and J.-L. Wang, Machine learning for high performance organic solar cells: Current scenario and future prospects, *Energy Environ. Sci.*, 2021, **14**, 90–105.

164 W. Sun, Y. Zheng, K. Yang, Q. Zhang, A. A. Shah, Z. Wu, Y. Sun, L. Feng, D. Chen, Z. Xiao, S. Lu, Y. Li and K. Sun, Machine learning-assisted molecular design and efficiency prediction for high-performance organic photovoltaic materials, *Sci. Adv.*, 2019, **5**, 4275.

